Chapter 13

Cruise Report: Sediment Collection from Orca and Pigmy Basins, Gulf of Mexico, and Analyses for Texture and Trace-Metal Concentrations, July 2002, PAGE 127 Campaign

James Flocks[1] and Peter Swarzenski[1]

Cruise report: Sediment collection from Orca and Pigmy Basins, Gulf of Mexico, and analyses for texture and trace-metal concentrations, July 2002, PAGE 127 campaign; chapter 13 in *Winters, W.J., Lorenson, T.D., and Paull, C.K., eds., 2007, Initial report of the IMAGES VIII/PAGE 127 gas hydrate and paleoclimate cruise on the RV* Marion Dufresne *in the Gulf of Mexico, 2–18 July 2002: U.S. Geological Survey Open-File Report 2004–1358.*

Introduction

The Mississippi River system, which drains almost half of the conterminous United States, ranks seventh among rivers worldwide for water discharge (580 cubic kilometers per year (km^3/yr)) and sixth for suspended-sediment discharge ($200x10^6$ metric tons per year (mt/yr)). Together, the Mississippi and Atchafalaya Rivers provide almost all of the freshwater influx to the Gulf of Mexico. The suspended-sediment load is composed predominantly of terrigenous clays and silts. A 3-year record of suspended-sediment load north of the Mississippi River Delta indicates that usually much more than 70 percent of the suspended load consists of particles that are less than 62 micrometers (μm) (4 phi (φ)) in size (Swarzenski, 2001). The silts are deposited along the periphery of the Mississippi River Delta, whereas the clays are transported offshore (Flocks and others, 2002; Walker and others, 2002). Fine particles, such as clay, are a primary transport mechanism for trace metals that adhere to the particle surface or are included interstitially within the silicate structure (Horowitz, 1991).

Trace-metal distribution in the Mississippi River Delta has been the subject of many research efforts (for example, DiMarco and others, 1986; Landrum, 1995; Trefry and others, 1995; Grant and Middleton, 1998). The extent to which the clay fraction distributes trace-metal constituents across the Gulf of Mexico is not entirely understood. During the Paleoceanography of the Atlantic and Geochemistry (PAGE) 127 campaign onboard the RV *Marion Dufresne*, sediment samples were collected along the continental slope several hundred miles southwest of the Mississippi River Delta. On July 8 and 9, 2002, two 11-meter-long box cores were deployed in two intraslope basins (Orca and Pigmy Basins) situated along the continental shelf in roughly 2,000 meters of water (fig. 1). Box core MD02-2550 was collected from Orca Basin and box core MD02-2553 from Pigmy Basin. The basins provide a sediment trap for pelagic and hemipelagic material and have been used in studies that address fluvial influence from the Mississippi River (Stearns and others, 1986; Raiswell and Canfield, 1998; Flower and others, 2004). Brine (in Orca Basin) and low-oxygen concentrations in the bottom waters provide a high preservation potential for organic material accumulating in the sediments. One objective of the survey was to collect and compare grain-size and trace-metal constituents from the basins with samples collected from the Mississippi and Atchafalaya River Deltas.

Methods

Coring and Sampling

Sediments were collected in a continuous, undisturbed 11-meter (m)-long core using the “Calypso3” box core developed for use on the research vessel (RV) *Marion Dufresne*. A

[1]USGS Center for Coastal and Watershed Studies, 600 4th St. South, St. Petersburg, FL 33701.

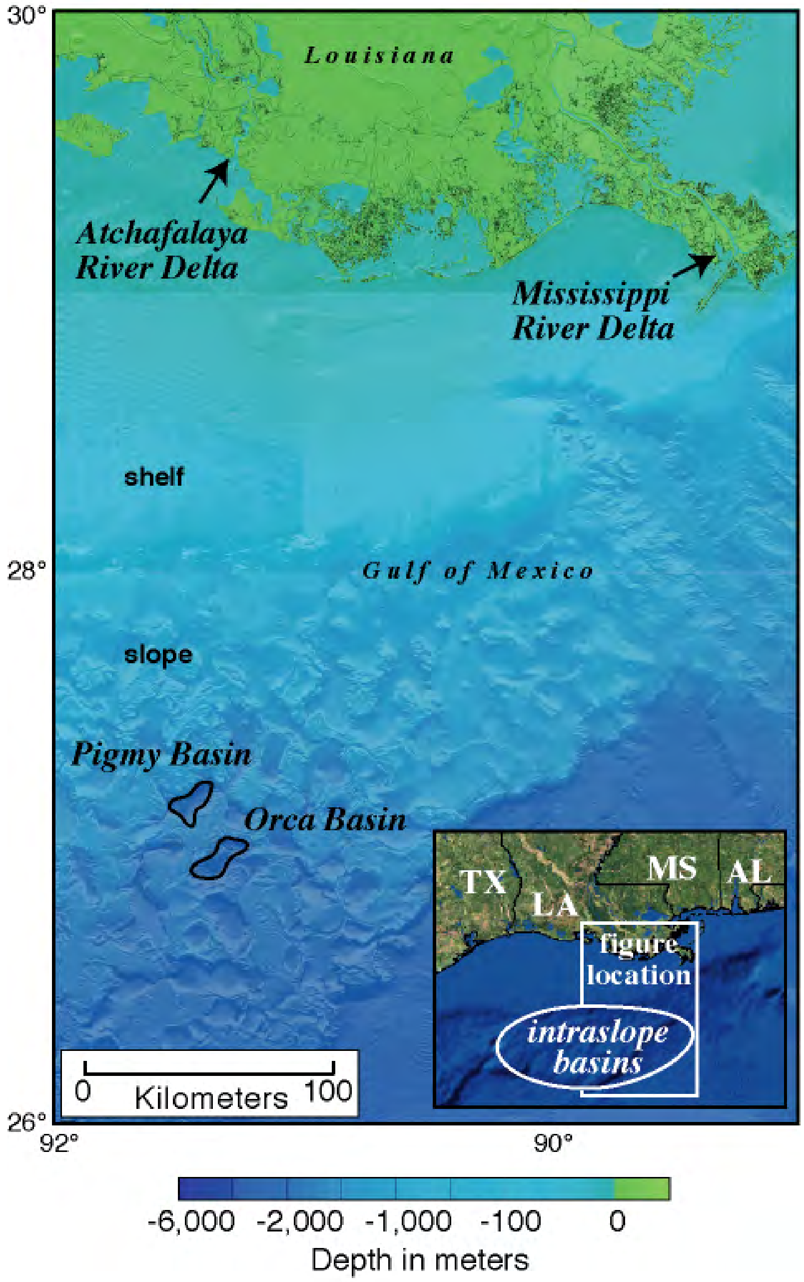

Figure 1. Locations of Orca and Pigmy intraslope basins and the Mississippi and Atchafalaya River Deltas, Gulf of Mexico. Bathymetric data from the National Geophysical Data Center (NGDC).

0.0625-square-meter (m^2) by 11-m-long steel box corer was attached to 2,400 kilograms (kg) of lead weight and lowered to the sea floor. Upon retrieval, one side of the box was removed to reveal the core. Plastic liners (8x13x155 centimeters (cm) were inserted longitudinally into the box core to subsample the sediment into four identical sections (fig. 2). For the purpose of this study, the first 2 m of one subcore was immediately sampled into 2.5-cm sections; each section was transferred to an individual plastic sampling cup and frozen.

Trace Metals

The subsamples were soaked in a 50-percent acetone-dH_2O mixture to remove organic material and facilitate wet sieving through a 63-μm screen. The resulting coarse and fine fractions were dried and weighed. The fine fraction was ground by mortar and pestle, and the coarse fraction was described and archived.

The fine fraction was further pulverized and analyzed using an inductively coupled plasma-optical emission spectrometer (ICP-OES) at a commercial laboratory (ACTLABS, Tucson, AZ). Elements measured by this method include aluminum (Al), calcium (Ca), cobalt (Co), copper (Cu), iron (Fe), potassium (K), magnesium (Mg), manganese (Mn), sodium (Na), phosphorous (P), nickel (Ni), lead (Pb), strontium (Sr), sulfur (S), titanium (Ti), yttrium (Y), vanadium (V) and zinc (Zn). Prior to analysis, the sediment samples were dissolved in acid to mobilize the trace metals into solution. “Near total” digestion employs HF, $HClO_4$, HNO_3, and HCl to get as much of the sample into solution as possible without fusing the sample (ACTLABS, written commun., 2002). Triplicates of two samples were analyzed to determine standard analytical error.

Grain Size

Textural analysis of sediment samples was performed at the U.S. Geological Survey (USGS) Center for Coastal Geology using a Coulter LS 200 particle-size analyzer. The LS 200 utilizes laser diffraction to measure size distribution of sedimentary particles between 0.4 μm and 2 millimeters (mm). Grain-size analyses were conducted by simulating the sizes that would be determined from standard ASTM 11-E sieves. For more information on this technique, see Kindinger and others (2001).

Scanning Electron Microscope (SEM)

The fine fraction of wet samples was pipetted into a micro-analysis vacuum filter and support assembly onto 0.2-mm polycarbonate filter pads. The filters were air-dried, mounted on aluminum stubs, and sputter coated with gold-palladium. The samples were then placed in a Hitachi 3500N

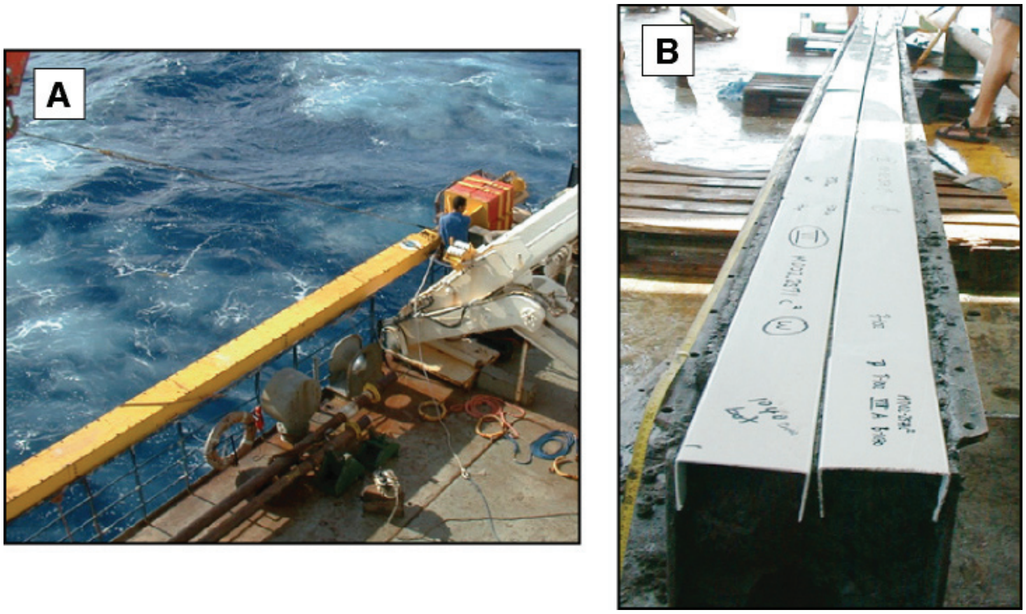

Figure 2. (A) Eleven-meter Calypso3 box core being deployed from the RV *Marion Dufresne*. (B) Opened box corer showing placement of subsampling tubes.

variable pressure scanning electron microscope (SEM) equipped with energy-dispersive spectroscopy (EDS). Samples were imaged using both secondary electron and backscatter electron detectors (atomic number differences). EDS was performed on several particles within each sample to determine relative elemental compositions.

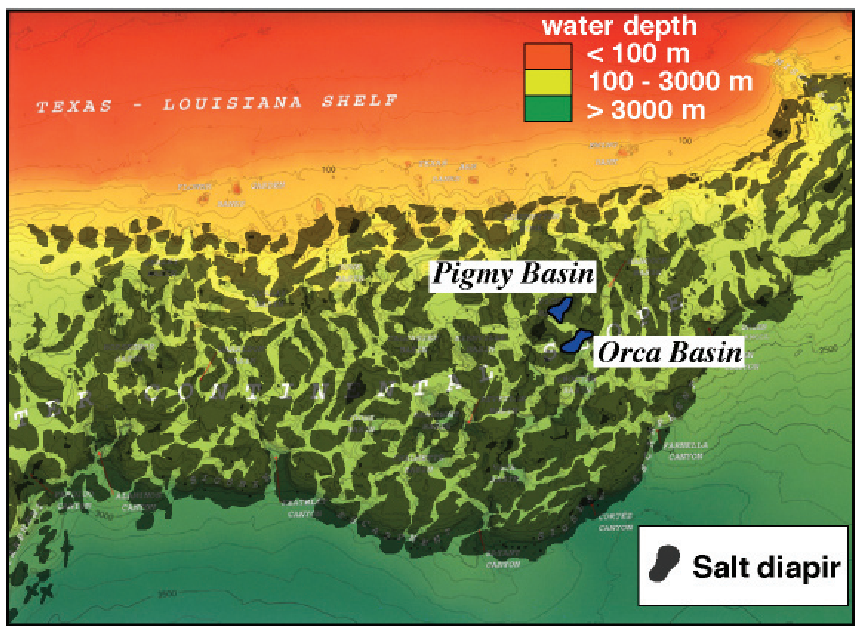

Figure 3. Bathymetric map showing positions of salt diapirs, northern Gulf of Mexico continental slope. Bathymetric data from NGDC, salt structure map from Bouma and others (1980). See figure 1 for locations of basins.

Discussion

Geology

The structure and topography of the slope that includes Pigmy and Orca Basins are controlled by salt diapirs (Bouma, 1981). Intrusion of these giant salt domes into the surficial sediments produced a topography similar to the Basin and Range Province of the Midwest of the United States (fig. 3), with dome rims protruding several hundred meters from the interdiapiric sea floor. The salt originates from Jurassic time and is overlain by shales of Tertiary age (Bouma and others, 1980). The shales are then overlain by a thick sequence of pelagic deposits and hemipelagic sediments of Pleistocene age associated with Mississippi River deposition.

Bouma and Coleman (1986) characterize several intraslope basin types relative to their previous geomorphology and subsequent diapiric construction: blocked-canyon, interdomal, and collapse basins. Pigmy Basin is an example of a blocked-canyon intraslope basin, which is defined as a former channel that has become blocked by upward or laterally moving diapirs. The channel effectively becomes dammed by the diapirs, terminating any basin infilling by bottom transport. Subsequent deposition in the basin is either by slumping along the periphery of the basin or through pelagic and hemipelagic accumulation. Orca Basin may not have started as a blocked canyon but is entirely isolated from outside currents by upward-moving diapirs. As a result, this example of an interdomal basin exhibits hypersaline and anoxic bottom waters, which preserve carbonate and organic material in the sediments (Tompkins and Shephard, 1979; Flower and others, 2004). Previous coring and seismic-profiling activities indicate that both basins contain a thick surficial sequence of sediments of Holocene to late Wisconsinan age (Bouma and Coleman, 1986; Jasper and Gagosian, 1990). Previous studies determined that the primary clay constituent in the top 3 m of sediment within Orca Basin is smectite, with lesser amounts of illite and kaolinite (Tompkins and Shephard, 1979).

Orca Basin Sediments (box core MD02-2550)

Box core MD02-2550 was acquired from the central portion of Orca Basin, in 2,249 m of water (fig. 4). A photomosaic of the core (fig. 5) shows over 6 m of light gray, faintly laminated clays, overlain by 2.5 m of black, laminated clay. The black color of the highly fluid surficial sediments represents FeS present in the hypersaline, anoxic muds that exist within the basin. The transition from gray to black muds presumably represents the beginning of anoxic conditions within the basin about 8,000 year before present (BP) (Trefry

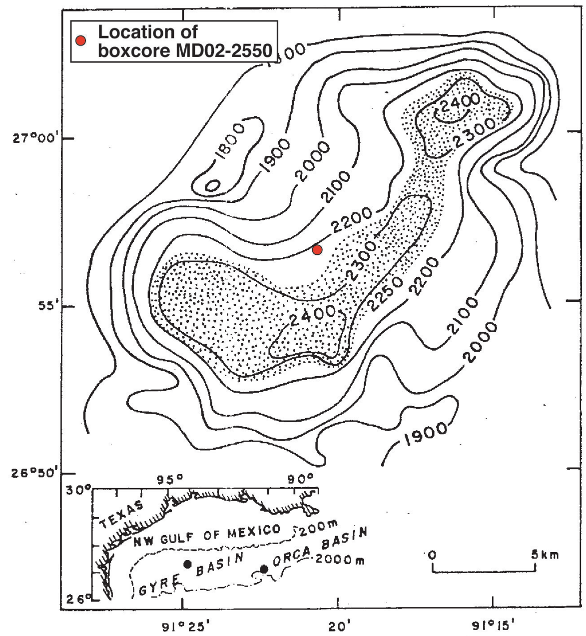

Figure 4. Bathymetric map of Orca Basin, from Bouma (1981), showing location of box core MD02-2550 (red dot).

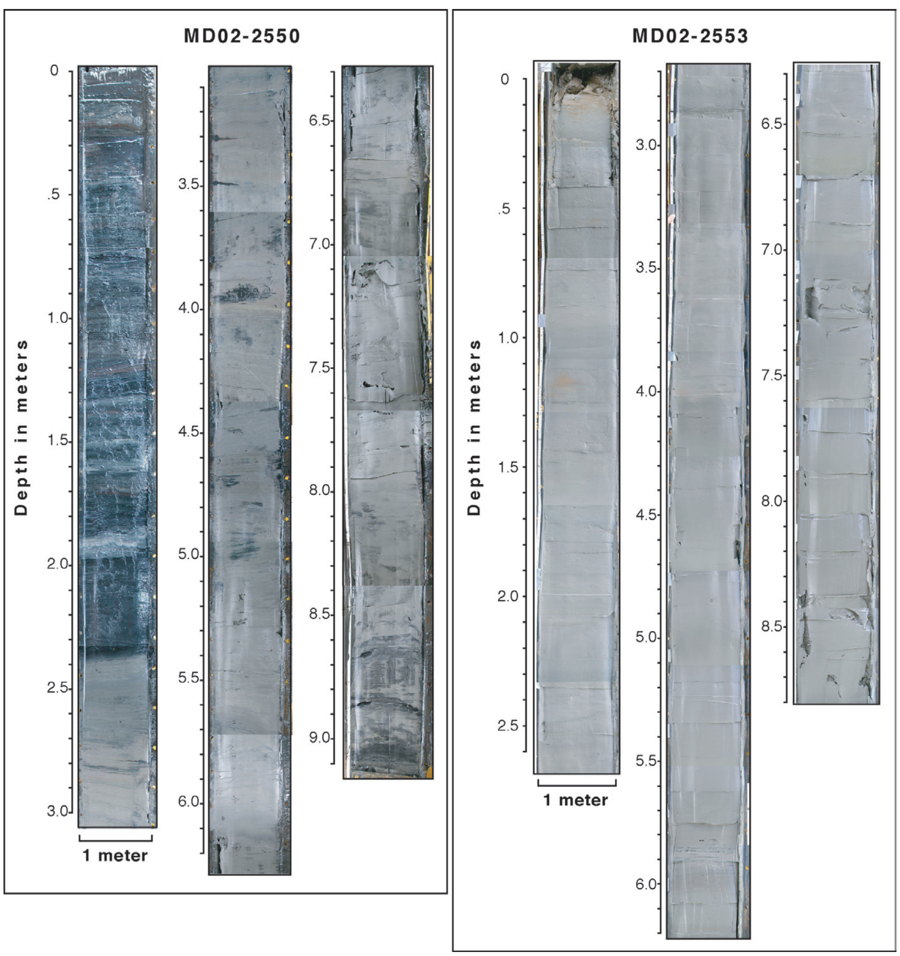

Figure 5. Photomosaic of box cores MD02-2550 (Orca Basin) and MD02-2553 (Pigmy Basin). Brightness differences and contrasting angles in laminations are due to camera angle and lighting.

and others, 1984). Hill and others (2004) estimate an average sediment accumulation rate of >50 cm per 1,000 year in the vicinity of the box core through radiocarbon dating from an adjacent piston core (MD02-2551). Their similar radiocarbon work on box core MD02-2550 indicates the middle Holocene may be missing (ca. 3 – 6.5 thousand years (ka)) between 175 and 190 cm (B. Flower, University of South Florida, oral commun., 2002). Throughout the core, signs of bioturbation are absent, and lamina thickness is variable. Evidence of gas vesicules occurs periodically.

A closeup of the several sieved fractions of the Orca Basin core shows an abundance of coccoliths, radiolarian tests, and spicules in a matrix of clay particles (fig. 6). Clay particles are identified by their silicate composition, determined using EDS, as are some trace amounts of quartz grains. Sand is not a major constituent in these samples; the coarse fraction was observed to contain mainly foraminifera and pteropods.

Grain-size analyses were performed every 10 cm over the top 3 m of the box core. Results show a predominance of clayey-silt throughout this section (fig. 7), with an overall coarsening upward in the core.

Trace-metal concentrations were measured in the top 2 m of the core. The results do not show marked variability in this section, with the top 0.5 m having the most consistency (fig. 8). Below 140 cm, there appears to be a slight increase in the concentration of some metals (Co, Mn, Ti, V, Y, Zn) and an increase in variability. This change is accompanied by a decrease in Na, which could indicate change in sediment texture if Na is a proxy for porosity. Selected trace-metal concentrations normalized to Al show some increase in the trace-metal component within the top 40 cm for Pb and Ni, relative to the rest of the core, but not a lot of variability (fig. 9). Deviations in the normalized trace-metal component at the base of the section (150–200 cm), in conjunction with the observation that approximately 20 cm may be missing, suggest that transport mechanisms may be active that are not evident in the upper 1 m of core. Selected trace-metal concentrations compared to samples acquired in the Mississippi River and Atchafalaya River Deltas indicate some variability (table 1). Average concentrations of Cu and Ni were similar to concentrations in the delta samples, whereas concentrations of Co, Pb, V, and Zn were lower.

Table 1. Average concentrations of selected trace metals from the basins compared to various locations around the northern Gulf of Mexico.

[*, peat and sand samples not included (intervals where > 50 percent of sample is > 36 micrometers (µm)) (Flocks and others, 2002); **, from Landrum (1995); ***, from Trefry and others (1995); —, not available]

Estuary/Basin	Co	Cu	Ni	Pb	V	Zn
Orca Basin (n=25)	6	21	23	14	78	48
Pigmy Basin (n=21)	11	37	35	16	137	89
Atchafalya Delta (n=42)*	10	19	25	20	95	76
Miss. Sub-deltas (n=27)* (n=27)*	10	20	25	25	83	77
Pass A Loutre (n=26)*	10	20	24	19	75	77
Miss. R. suspended sed***	—	—	41	36	132	—
St. Bernard delta regtion**	29	19	22	26	47	120
Apalachicola Bay**	18	37	—	—	79	57
Barataria Basin**	25	22	26	18	23	98
Beaumont Area**	—	20	17	—	—	108
Corpus Christi**	—	15	15	17	—	93
Galveston Area**	—	27	22	34	—	62
Mississippi Sound**	13	20	—	—	80	74
Mobile Bay**	15	31	—	—	88	120
Pensacola Bay**	8	31	—	—	75	86
Perdido Bay**	27	46	—	—	49	161
Pontchartrain Estuary**	9	23	17	81	78	78

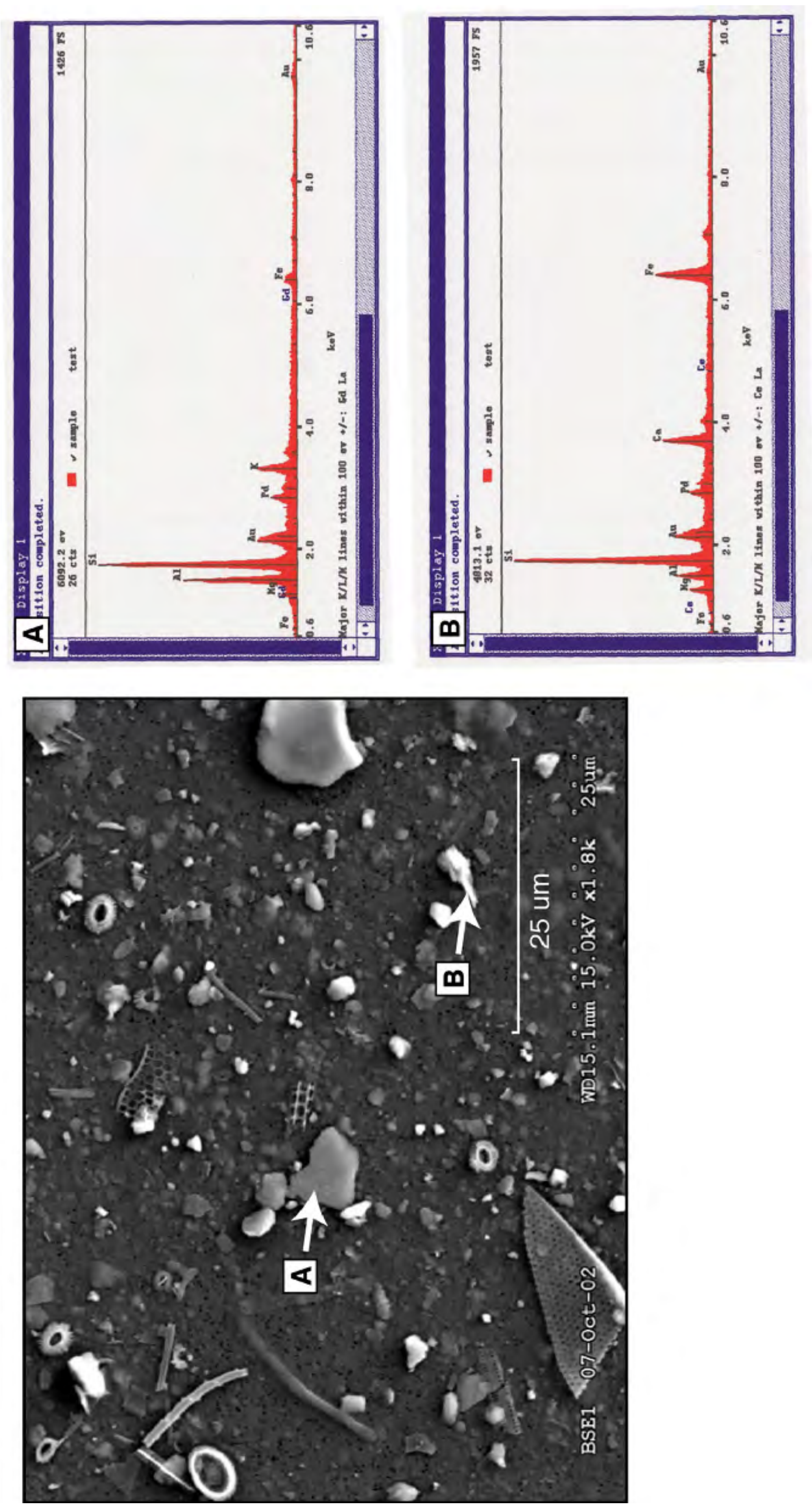

Figure 6. Scanning Electron Microscopy (SEM) image of particles less than 6 phi (φ); silt size) from box core MD02-2550, showing pelagic and hemipelagic material. Selected clay particles were analyzed for elemental composition using energy-dispersive spectroscopy (EDS; right), showing silicate composition and associated major cations. More SEM images with EDS analysis are included in the appendix to this chapter.

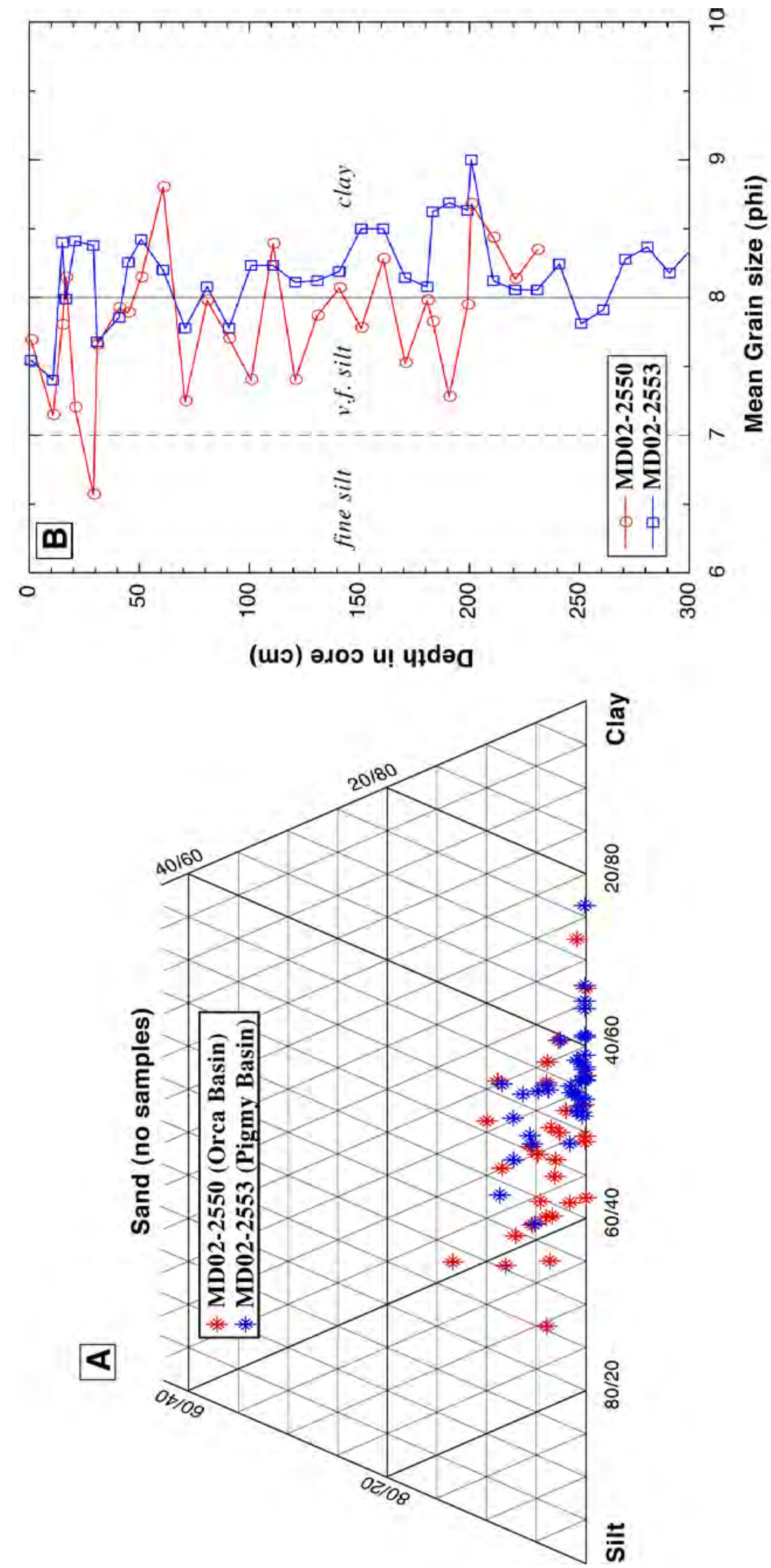

Figure 7. Grain-size analyses showing (A) distribution of samples and (B) trend and predominance of clay-size sediments.

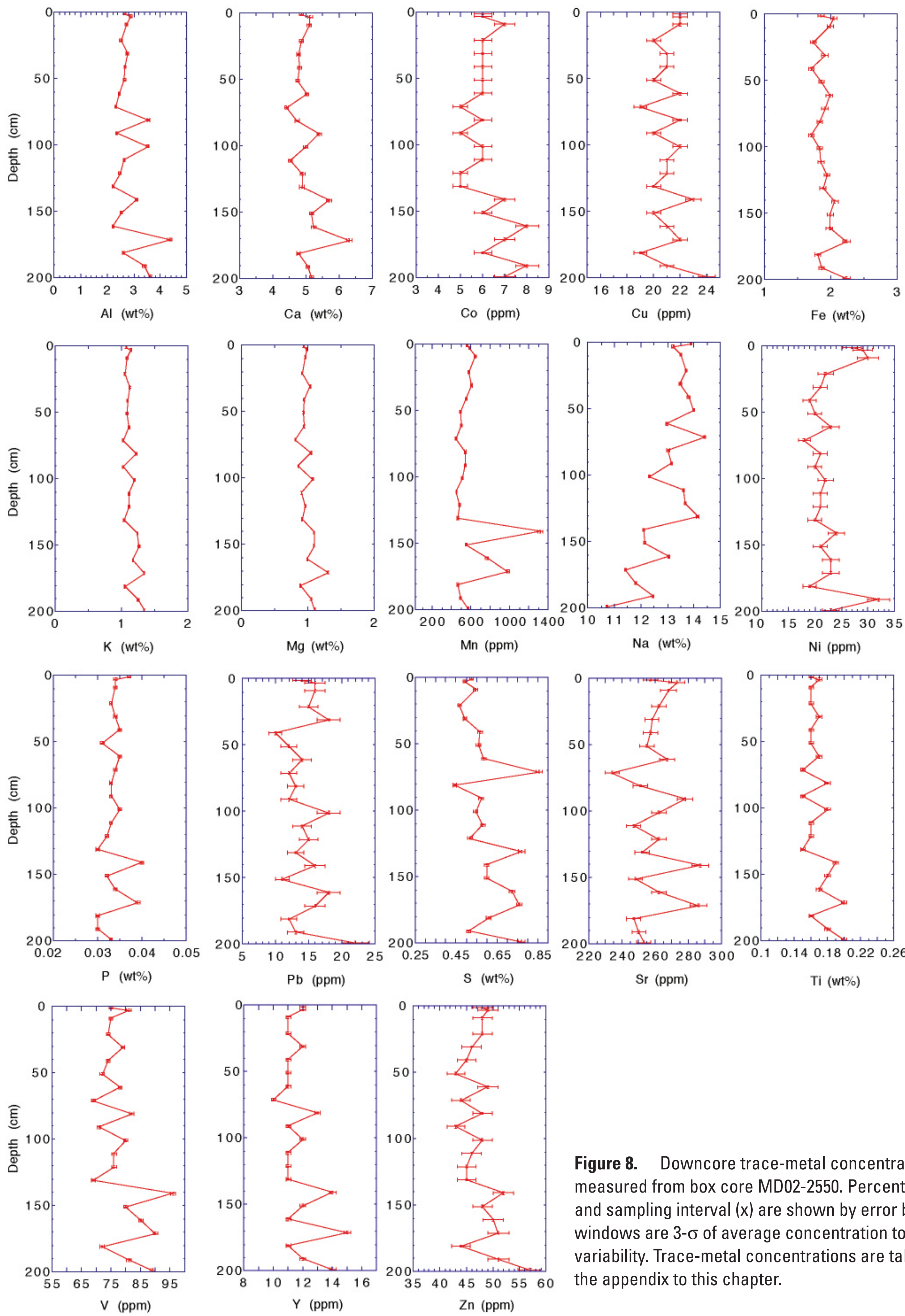

Figure 8. Downcore trace-metal concentrations measured from box core MD02-2550. Percent error (y) and sampling interval (x) are shown by error bars. Graph windows are 3-σ of average concentration to show variability. Trace-metal concentrations are tabulated in the appendix to this chapter.

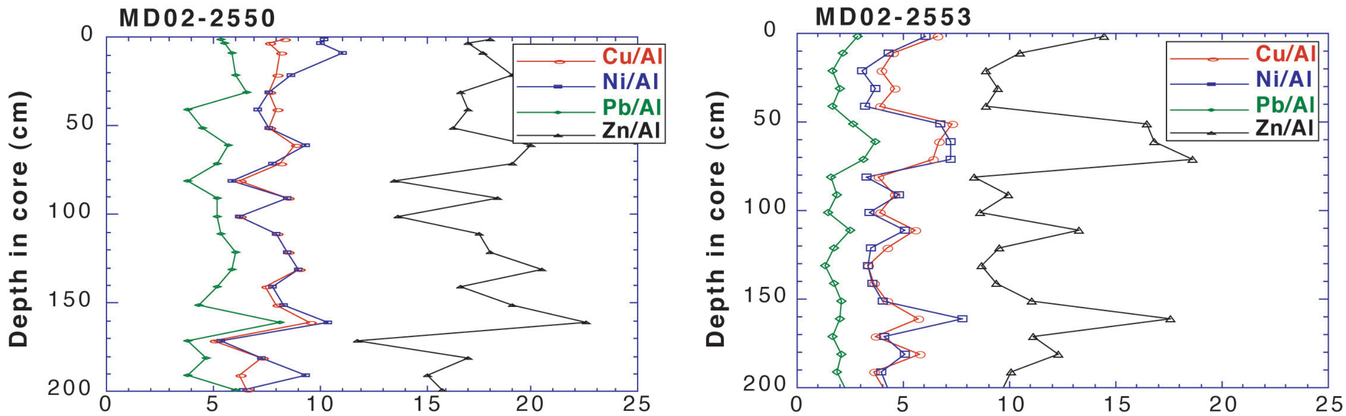

Figure 9. Selected trace-metal concentrations normalized to Al to reflect possible deviations from estimated background (environmental) conditions.

Pigmy Basin Sediments (box core MD02-2553)

Pigmy Basin has a maximum depth of about 2,240 m, with a sill depth of less than 1,700 m (fig. 10). Box core MD02-2553 was acquired in the central portion of the basin. Photographs of the sediments show gray, generally massive to faintly laminated muds throughout the length of the core (fig. 5). Black shading related to accumulation of organic material occurs throughout the core, and distinct concentrations of foraminifera occur at 65, 125, 127, 313, 315, and 442 cm downcore. There is no evidence of bioturbation or other physical disturbance to the sediments.

Comparison of SEM images between Orca and Pigmy Basins shows Pigmy sediments contain a similar amount of coccoliths, but no pteropods (figs. 6, 11); the basin has a lower preservation potential for aragonite. Poore and others (2004) estimate an average sediment accumulation rate of 50 cm per 1,000 years using AMS radiocarbon dating of planktonic foraminifera in the top 2 m of the core. However, through comparison with tree-ring dating, Poore and others (2005) suggest that small variations in sediment accumulation may exist. Variability in sedimentation may be due in part to a migrating source of fluvial clays. Throughout the 4,000 years of accumulation represented by this section of core, the primary discharge of the Mississippi River has varied in proximity to the basin by over 100 kilometers (km). Over that time, delta switching changed the course of the Mississippi River from the St. Bernard complex west to the Lafourche Delta, and then east to its current configuration (Frazier, 1967; Levin, 1991). Examination of the clay particles within the sample using EDS shows silicates with the presence of Al, K, Ca, Mn, and Fe (fig. 11).

Trace-metal concentrations within Pigmy Basin are consistently higher than those found in Orca Basin (with the understandable exception for Na and S) and other areas of the Mississippi River Delta (table 1). There is close correlation in trend between Ca, Sr, Al, and Y downcore (fig. 12). A less obvious, opposite trend can be seen in Ni, Pb, Ti, and Zn. This variance becomes more obvious when the latter constituents are normalized to Al (fig. 9). The increase in these constituents shown in figure 9 may be related to an enhanced terrestrial component.

Grain-size analysis indicates the sediments within Pigmy Basin are composed almost entirely of clay-size particles (fig. 7), with a smaller average diameter than sediments collected from Orca Basin. Mean grain size shows minimal variability around the silt/clay boundary (fig. 7), with possibly a slight coarsening-upward trend.

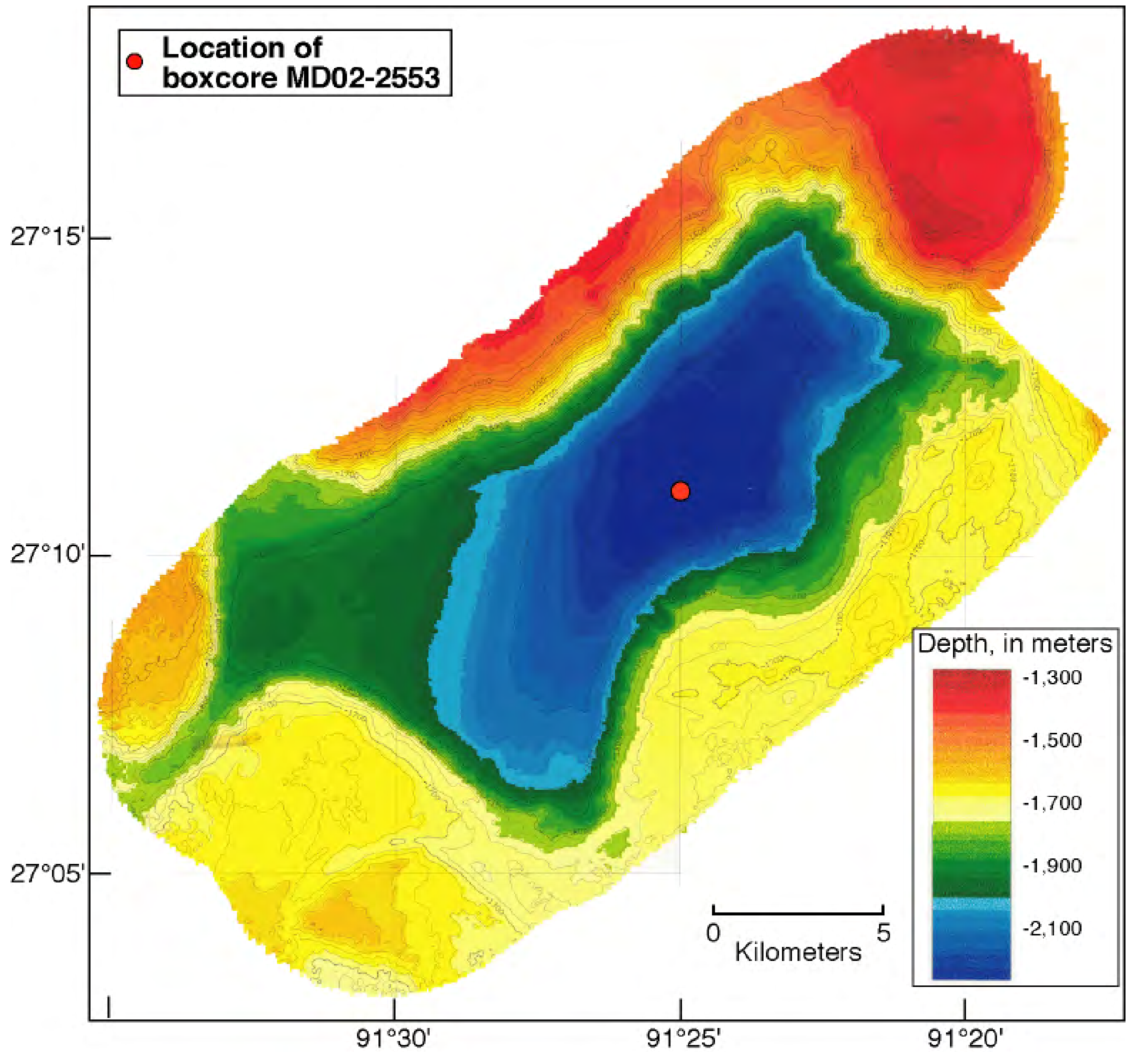

Figure 10. Bathymetric map of Pigmy Basin. Contours were generated from a geophysical survey conducted during the Paleoceanography of the Atlantic and Geochemistry (PAGE) 127 campaign. Location of box core MD02-2553 shown (red dot). Location of Pigmy Basin is shown in figure 1.

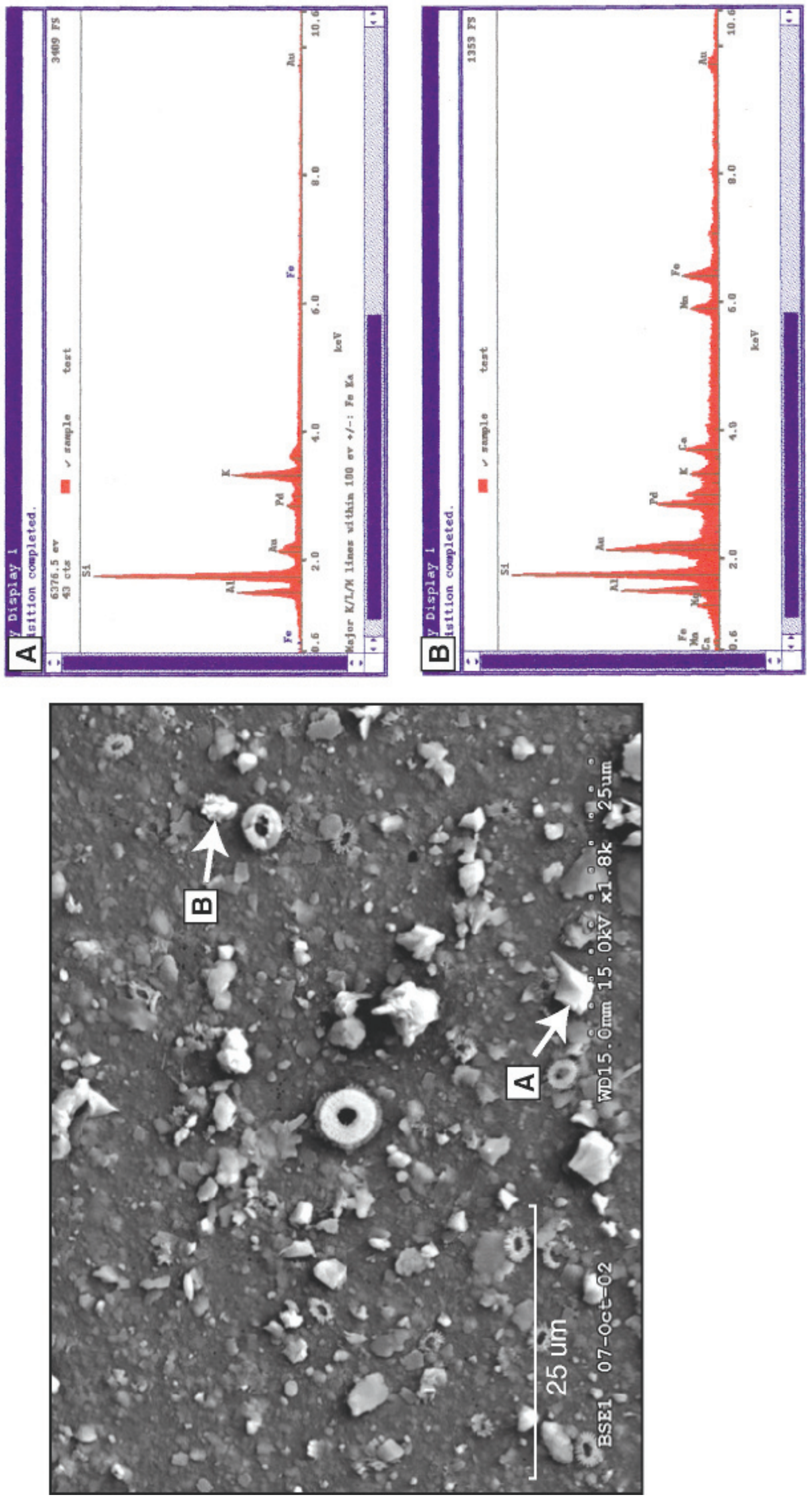

Figure 11. Scanning Electron Microscopy (SEM) image of particles less than 6 phi (θ); silt size) from box core MD02-2553, showing pelagic and hemipelagic material. Selected clay particles were analyzed for elemental composition using energy-dispersive spectroscopy (EDS; right), showing silicate composition and associated major cations. More SEM images with EDS analysis are included in the appendix to this chapter.

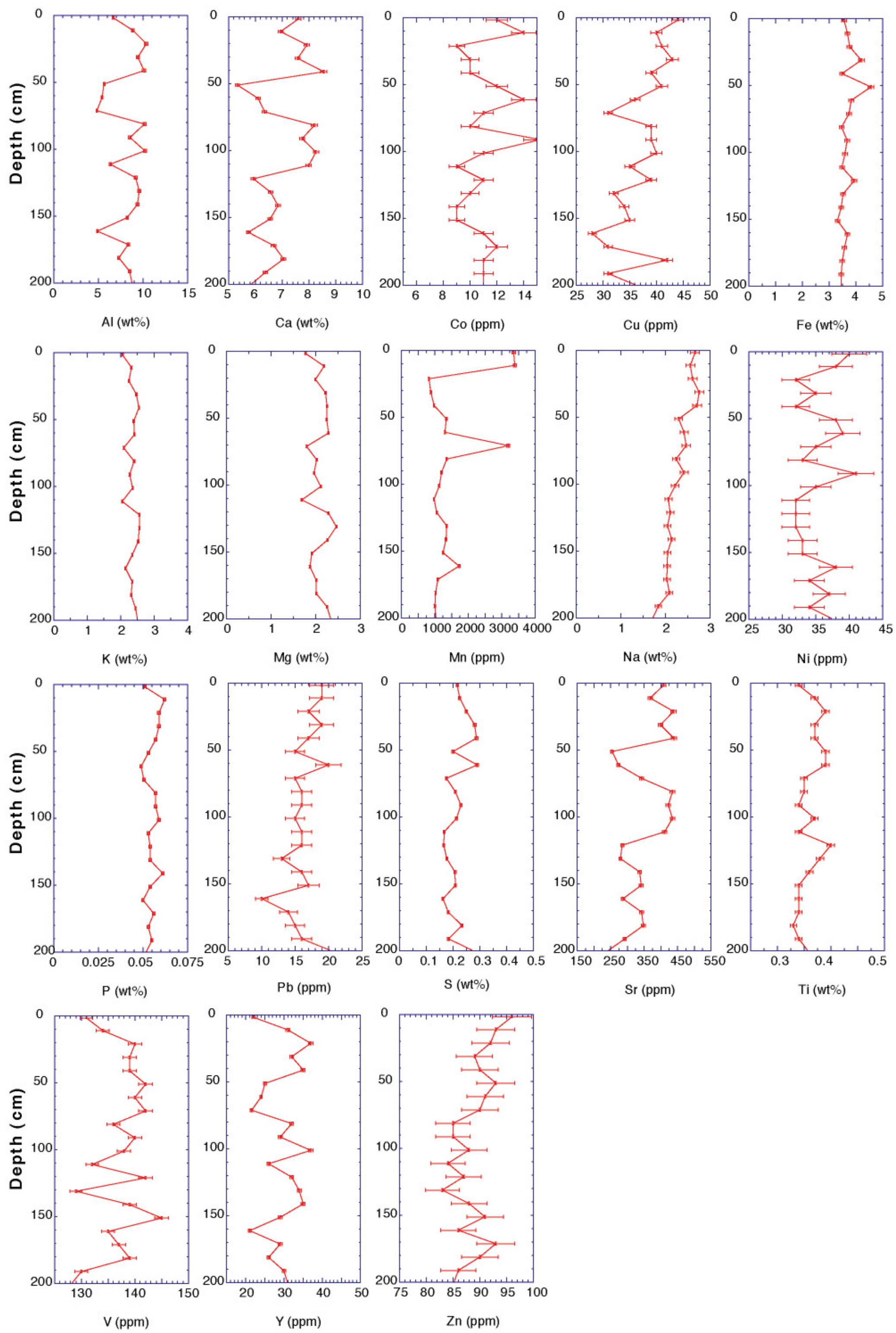

Figure 12. Downcore trace-metal concentrations measured from box core MD02-2553. Percent error (y) and sampling interval (x) are shown by error bars. Graph windows are 3-σ of average concentration to show variability. Trace-metal concentrations are tabulated in the appendix to this chapter.

Conclusion

Textural analyses of sediments collected from Orca and Pigmy Basins indicate the sediments to be well-sorted very fine silts and clays. There is little variability downcore in the top 2 m, with perhaps a slight coarsening upward in both basins. Sediments collected from Pigmy Basin have a smaller average grain size, about the 8-phi class, than Orca Basin sediments. Sediments from Pigmy Basin can be described as silty-clay, and those from Orca Basin can be characterized as clayey-silt. SEM imagery from the sediments show both basins contain abundant foraminifera. Orca Basin sediments contain abundant pteropods, whereas the Pigmy Basin sediments do not. EDS analysis through SEM show the clay particulate to contain the major cations (Ca, Mn, Fe, and Al), although clay species cannot be determined at this time. Some minor quartz and carbonate material were also found.

Trace-metal analysis demonstrates little variability in the top 2 m of sediment. Subtle trends in both basins indicate correlation in some constituents (for example, Al, Ca, Sr, and Y), possibly coincident with a mass balance in others (for example, Ni, Pb, Ti, and Zn). These variances may reflect an inconsistent fluvial component. The low-oxygen and hypersaline conditions in Orca Basin correspond to higher S and Na concentrations in the Orca sediments, and metal concentrations in Pigmy Basin are consistently higher than in Orca Basin. Lower sediment concentrations of certain soluble metals, such as Fe and Mn in Orca Basin as compared to Pigmy Basin, may reflect remobilization and precipitation processes that occur above the sea floor, in the brine, and in seawater columns (Trefry and others, 1984).

Table 1 lists trace-metal concentrations measured within various coastal and estuarine sediments from the northern Gulf of Mexico. The sediments were collected by surface grab and shallow sediment cores, and reflect the modern distribution of trace metals within the coastal environment. Compared to these analyses, the sediments from Orca Basin indicate similar or lower concentrations, whereas those from Pigmy Basin indicate significantly higher values (table 1). Comparison of the abundance of clay within the samples to selected trace metals (Cu, Pb) across these environments indicates a possible correlation. The higher clay fraction in the shelf-slope basin cores supports a higher concentration of Cu than in various facies of deltaic sediments (fig. 13). Although Cu and other metals may have an affinity for clay particulate, the Pb profile in the figure shows that correlation between trace-metal concentration and percentage of fine-grained material is not consistent. This suggests that Pb may have alternate or more complex transport mechanisms.

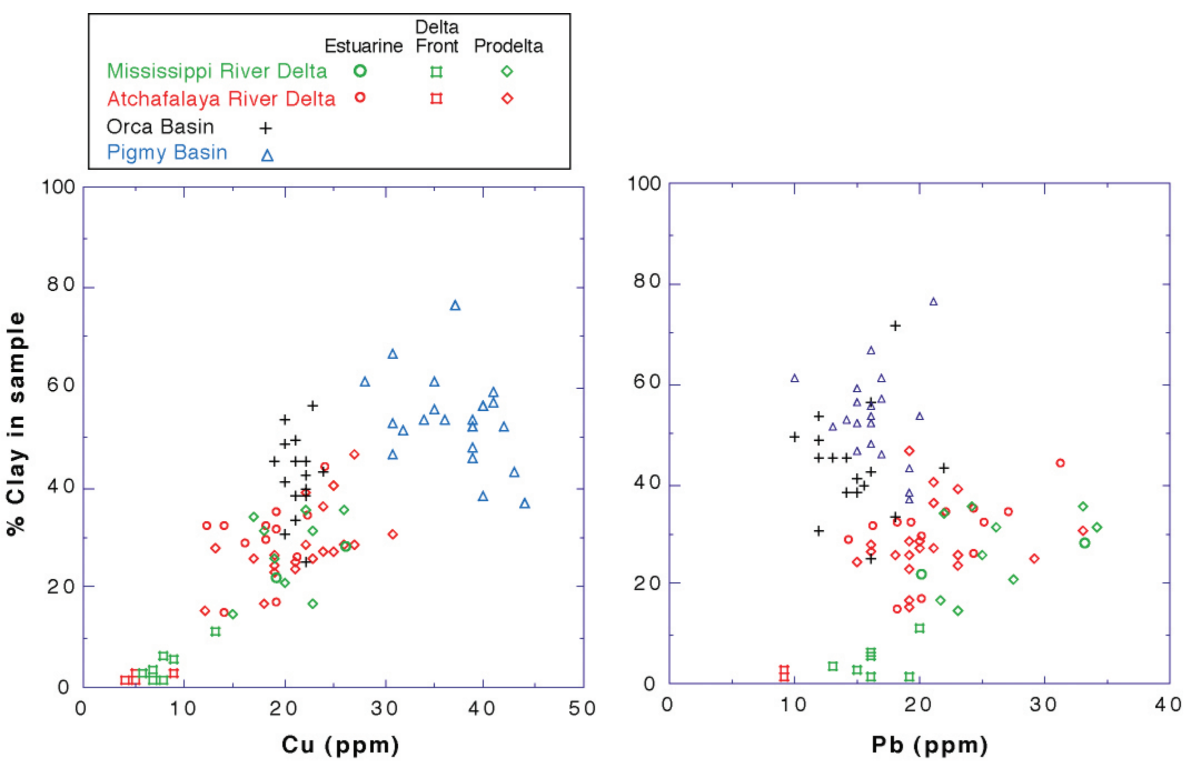

Figure 13. Clay-size constituent in relation to selected trace-metal (Cu, Pb) concentrations in samples collected from various environments in the northern Gulf of Mexico, from Flocks and others (2002). Samples from the deltas are divided into depositional facies associated with transgressive-phase delta development.

Acknowledgments

The authors thank Bill Waite and Pat Hart for assistance during the cruise and for contributing digital images and maps, Noreen Buster for the SEM analyses, and Nick Ferina and Chandra Dreher for sample preparation and grain-size analyses. Comments and review from Dick Poore, Brian Bossak, and Barbara Lidz are greatly appreciated.

References

Bouma, A., 1981, Submarine canyon-fan systems in a diapirically controlled area, Gulf of Mexico—sedimentary Environments of the North Atlantic during the Quaternary: Proceedings of the National Council for Scientific Research (NCSR) International Colloquium no. 325, 18 p.

Bouma, A., and Coleman, J., 1986, Intraslope basin deposits and relation to continental shelf, northern Gulf of Mexico: American Association of Petroleum Geologists Bulletin, v. 70, no. 9, p. 1178.

Bouma, A., Martin, R., and Bryant, W., 1980, Shallow structure of upper continental slope, central Gulf of Mexico: Proceedings, Offshore Technology Conference, v. 4, no. 12, p. 583–592.

DiMarco, M., Ferrel, R., Jr., and Tye, R., 1986, Clay mineralogy of Cubits Gap crevasse splay, Mississippi Delta: Gulf Coast Association of Geological Societies Transactions, v. 36, p. 441–447.

Flocks, J., Kindinger, J., Ferina, N., and Dreher, C., 2002, Sediment-hosted contaminants and distribution patterns in the Mississippi and Atchafalaya River Deltas: Gulf Coast Association of Geological Societies Transactions, v. 52, p. 277–289.

Flower, B., Hastings, D., Hill, H., and Quinn, T., 2004, Phasing of deglacial warming and Laurentide Ice Sheet meltwater in the Gulf of Mexico: Geology, v. 32, no. 7, p. 597–600.

Frazier, D., 1967, Recent deltaic deposits of the Mississippi River—their development and chronology: Gulf Coast Association of Geological Societies Transactions, v. 17, p. 287–315.

Grant, A., and Middleton, R., 1998, Contaminants in sediments—using robust regression for grain-size normalization: Estuaries, v. 21, p. 197–203.

Hill, H., Flower, B., Hollander, D., and Quinn, T., 2004, Evidence for oceanic/continental climate linkages during freshwater inputs to the Gulf of Mexico: EOS Transactions, American Geophysical Union, v. 47, no. 85, Fall Meeting Supplemental Abstract PP44A-07.

Horowitz, A., 1991, A primer on sediment-trace element chemistry: Boca Raton, Florida, Lewis Publishers, 136 p.

Jasper, J., and Gagosian, R., 1990, The sources and deposition of organic matter in the Late Quaternary Pigmy Basin, Gulf of Mexico: Geochimica et Cosmochimica Acta, v. 54, p. 1117–1132.

Kindinger, J., Flocks, J., Kulp, M., Penland, S., and Britsch, L., 2001, Sand resources, regional geology and coastal processes for the restoration of the Barataria barrier shoreline: U.S. Geological Survey Open-File Report 01–384, 69 p.

Landrum, K., 1995, Trace-metal variability of estuarine sediments, St. Benard geomorphic region, Louisiana: Gulf Coast Association of Geological Societies Transactions, v. 65, p. 365–370.

Levin, D., 1991, Transgressions and regressions in the Barataria Bight region of coastal Louisiana: Gulf Coast Association of Geological Societies Transactions, v. 41, p. 408–431.

Poore, R., Pavich, M., and Grissino-Mayer, H., 2005, Record of the North American southwest monsoon from Gulf of Mexico sediment cores: Geology, v. 33, no. 3, p. 209–212.

Poore, R., Quinn, T., and Verardo, S., 2004, Century-scale movement of the Atlantic intertropical convergence zone linked to solar variability: Geophysical Research Letters, v. 31, L12214, 4 p.

Raiswell, R., and Canfield, D., 1998, Sources of iron for pyrite formation in marine sediments: American Journal of Science, v. 298, no. 3, p. 219–245.

Stearns, S., Tieh, T., and Presley, B., 1986, Mineralogy and incipient diagenesis in sediments of Pigmy Basin, northern Gulf of Mexico: American Association of Petroleum Geologists Bulletin, v. 70, no. 5, p. 652.

Swarzenski, P., 2001, Evaluating basin/shelf effects in the delivery of sediment-hosted contaminants in the Atchafalaya and Mississippi River Deltas: U.S. Geological Survey Open-File Report 01–215, accessed October 17, 2006, at *http://gulfsci.usgs.gov/missriv/reports/ofrshelf/index.html*

Tompkins, R., and Shephard, L., 1979, Orca Basin—depositional process, geotechnical properties and clay mineralogy of Holocene sediments within an anoxic hypersaline basin, northwest Gulf of Mexico: Marine Geology, v. 33, p. 221–238.

Trefry, J., Naito, K., Trocine, R., and Metz, S., 1995, Distribution and bioaccumulation of heavy metals from produced water discharges to the Gulf of Mexico: Water Science Technology, v. 32, no. 2, p. 31–36.

Trefry, J., Presley, B., Keeney-Kennicutt, W., and Trocine, R., 1984, Distribution and chemistry of manganese, iron, and suspended particulates in Orca Basin: Geo-Marine Letters, v. 4, p. 125–130.

Walker, N., Roberts, H., Stone, G., Bentley, S., Huh, O., Sheremet, A., Rouse, L., Inoue, M., Welsh, S., Hsu, S., and Myint, S., 2002, Satellite-based assessment of sediment transport, distribution and resuspension associated with the Atchafalaya River discharge plume: Gulf Coast Association of Geological Societies Transactions, v. 52, p. 967–973.

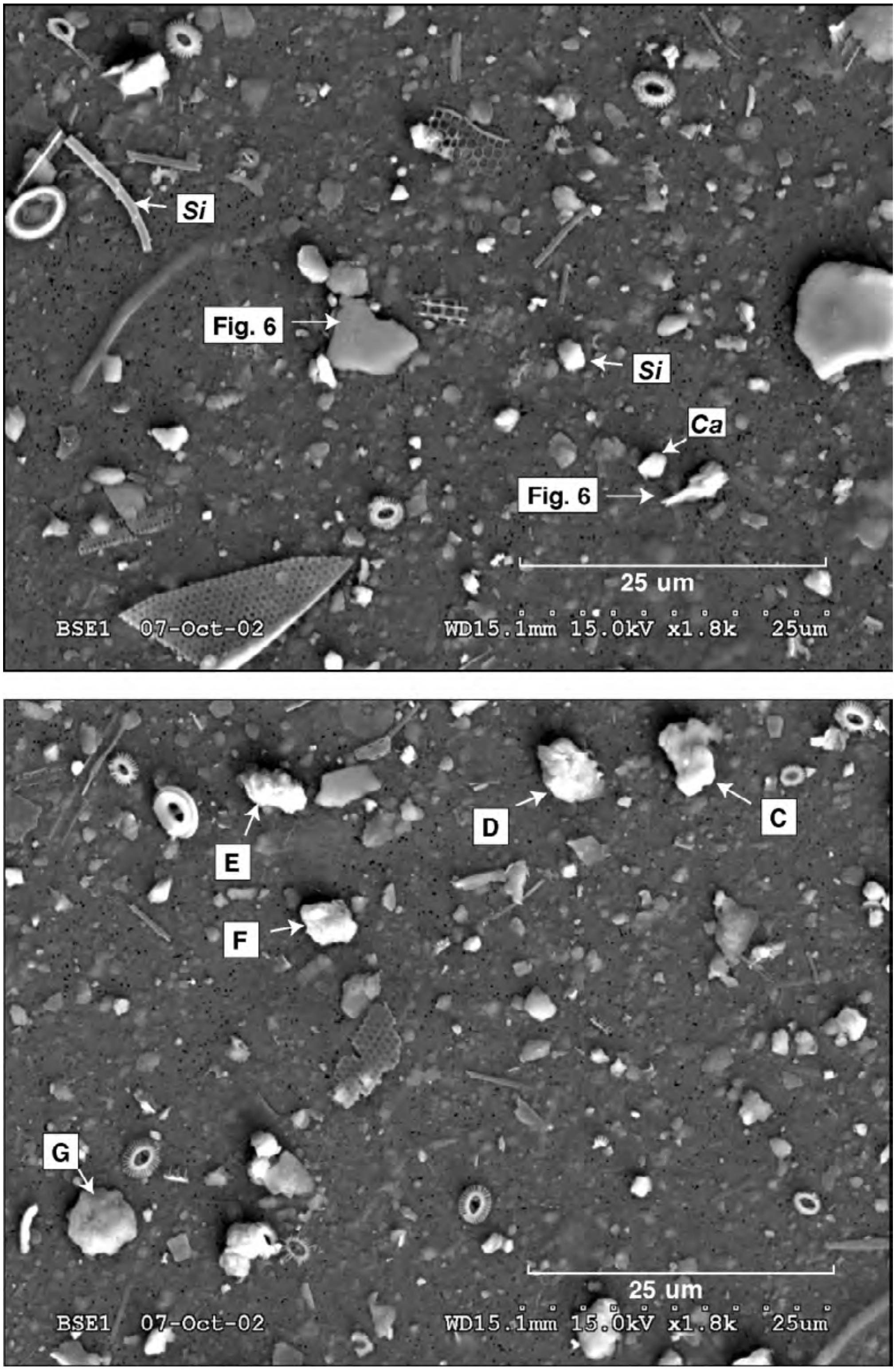

Attachment 1. SEM images of a <6-phi sample from box core MD02-2550 (Orca Basin). Letters mark particles that have been analyzed using EDS, results shown in subsequent attachments. Italicized letters list element (Si = silicon, Ca = calcium, etc.) found in particle.

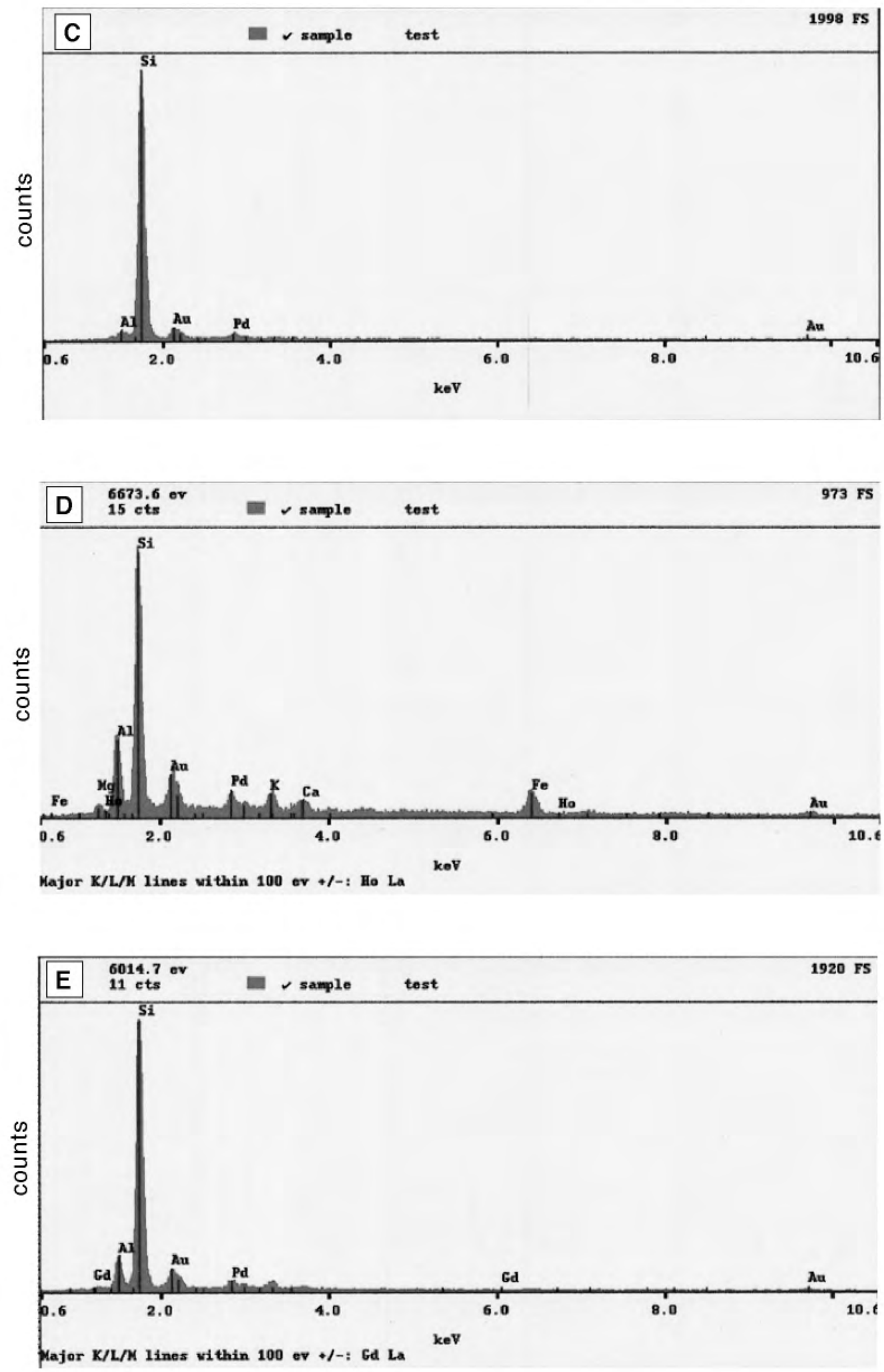

Attachment 2. EDS spectrum showing relative elemental composition of particles marked in Attachment 1. X-axis shows energy level, y-axis represents counts. The samples were coated with Au/Pd.

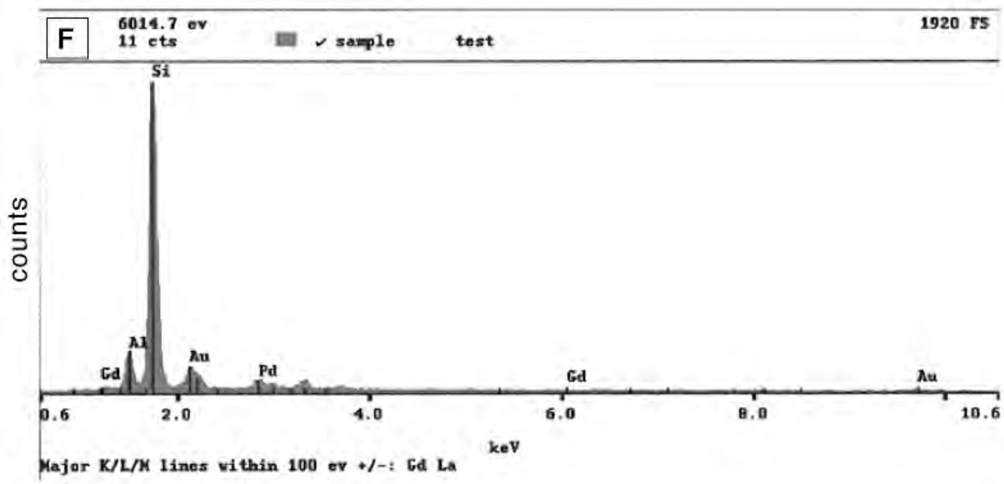

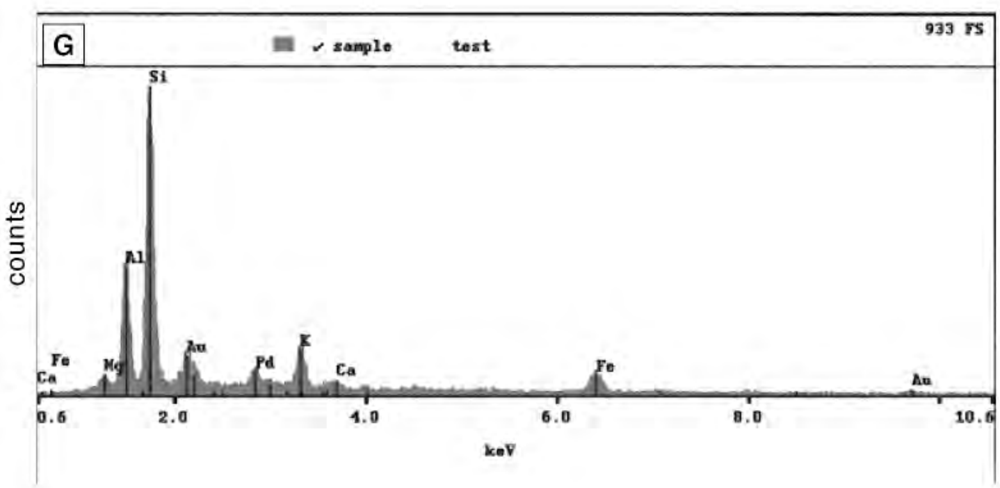

Attachment 3. EDS spectrum showing relative elemental composition of particles marked in Attachment 1. X-axis shows energy level, y-axis represents counts. The samples were coated with Au/Pd.

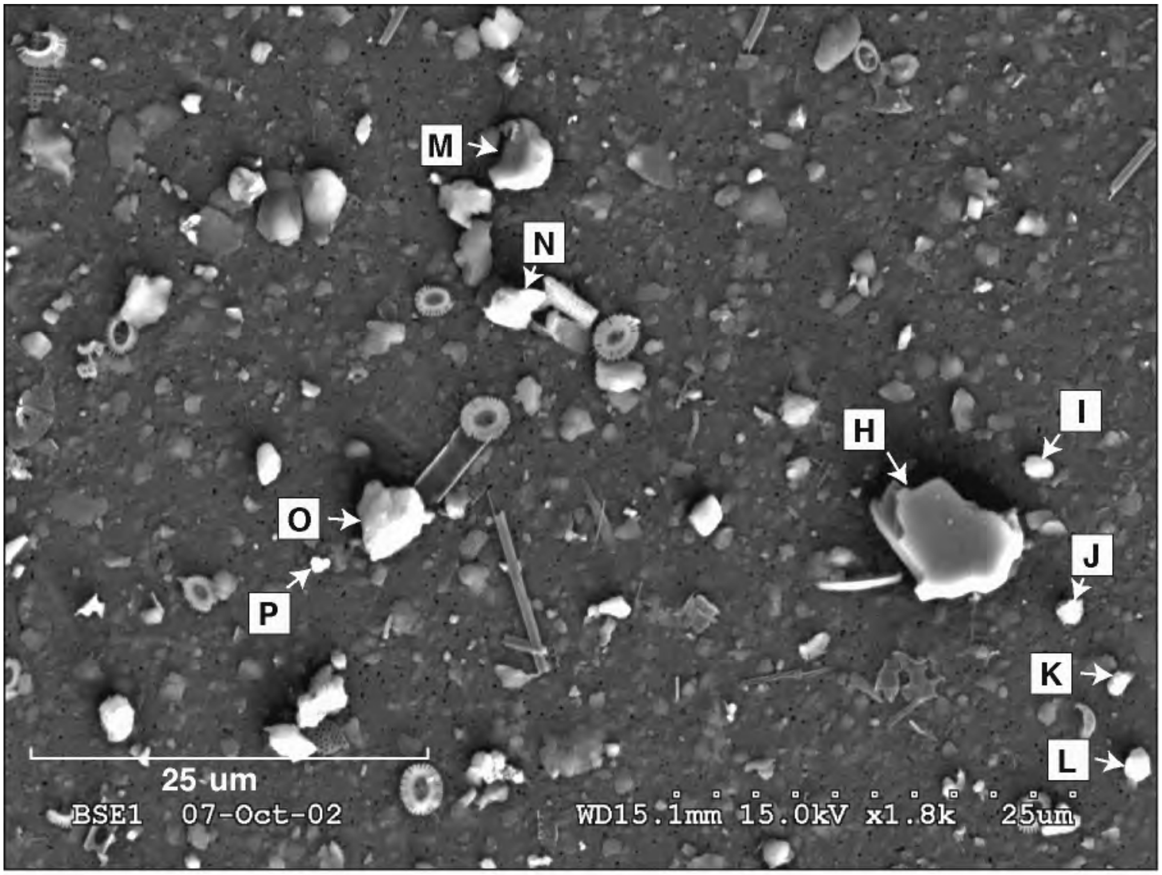

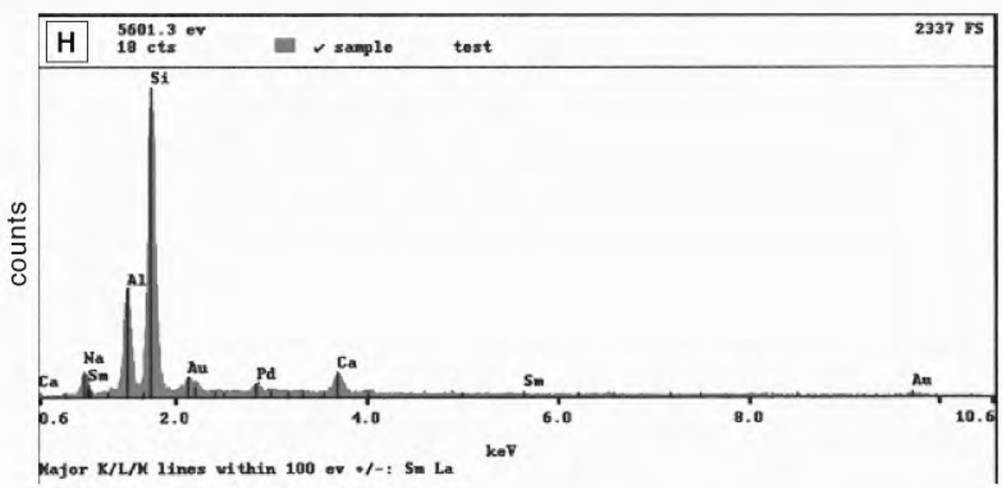

Attachment 4. Top: SEM images of a <6-phi sample from box core MD02-2550 (Orca Basin). Letters mark particles that have been analyzed using EDS, results shown in subsequent attachments. Bottom: EDS spectrum showing relative elemental composition of particles "H" shown in above image. X-axis shows energy level, y-axis represents counts. The samples were coated with Au/Pd.

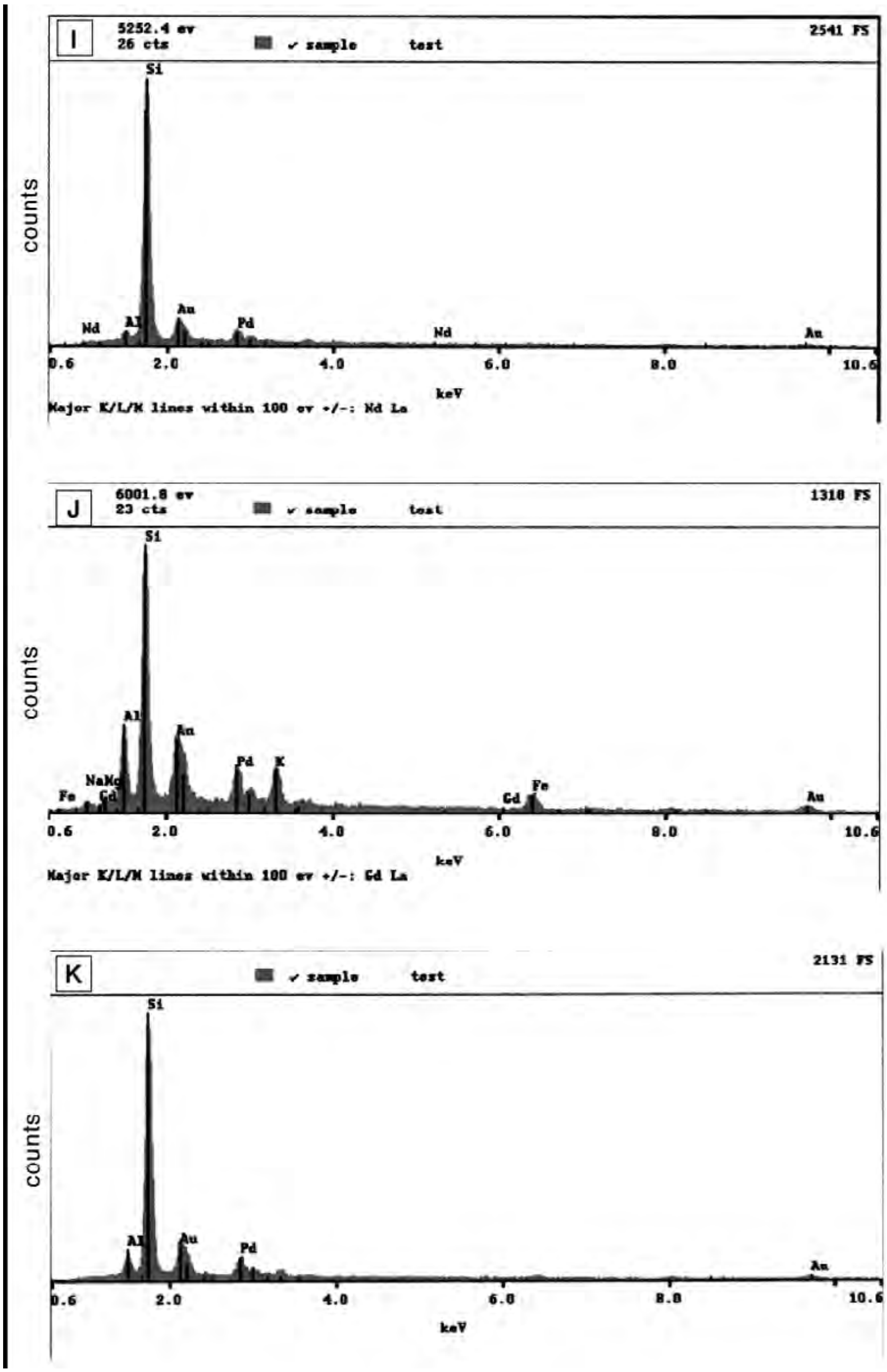

Attachment 5. EDS spectrum showing relative elemental composition of particles marked in Attachment 4. X-axis shows energy level, y-axis represents counts. The samples were coated with Au/Pd.

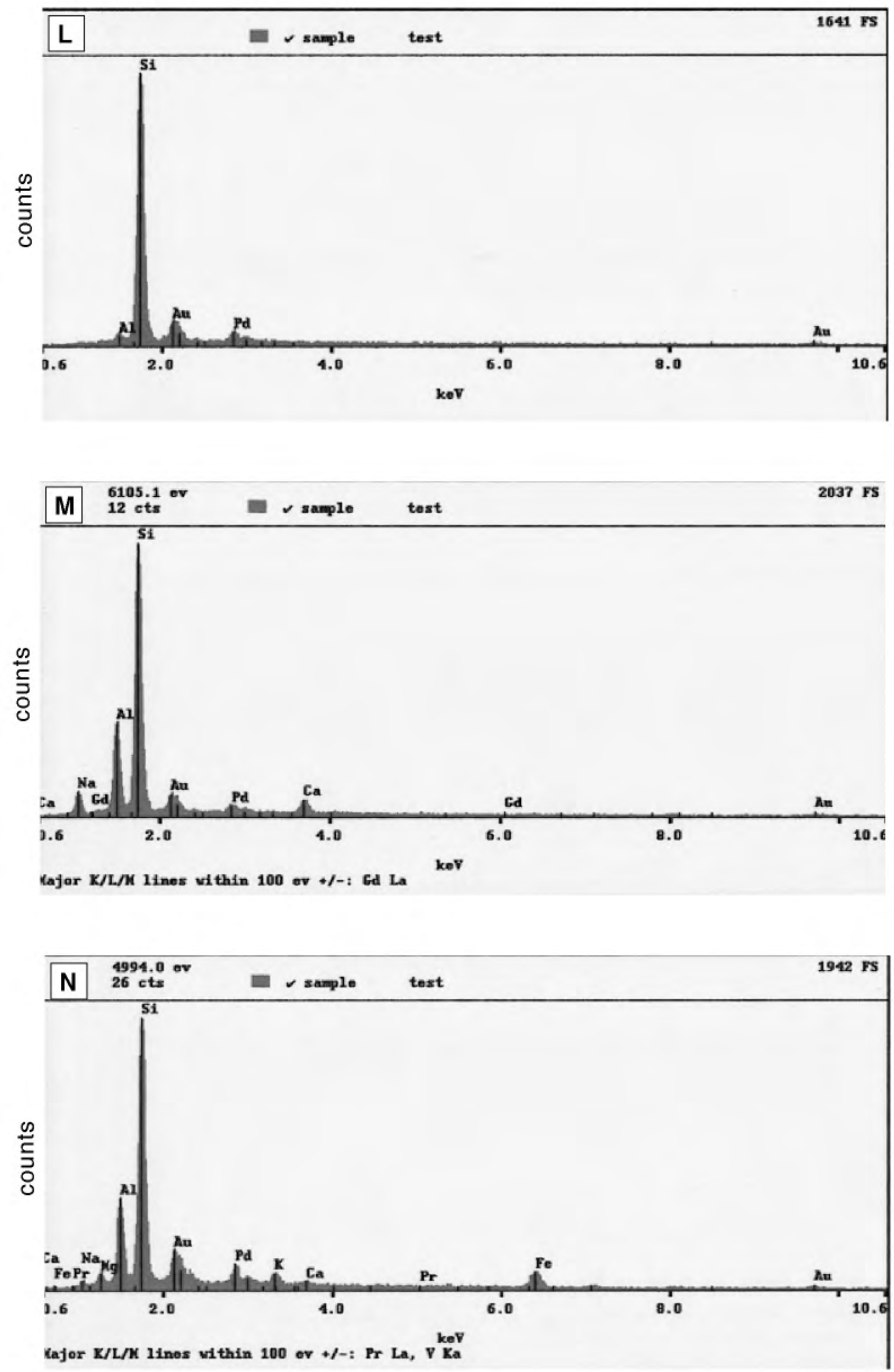

Attachment 6. EDS spectrum showing relative elemental composition of particles marked in Attachment 4. X-axis shows energy level, y-axis represents counts. The samples were coated with Au/Pd.

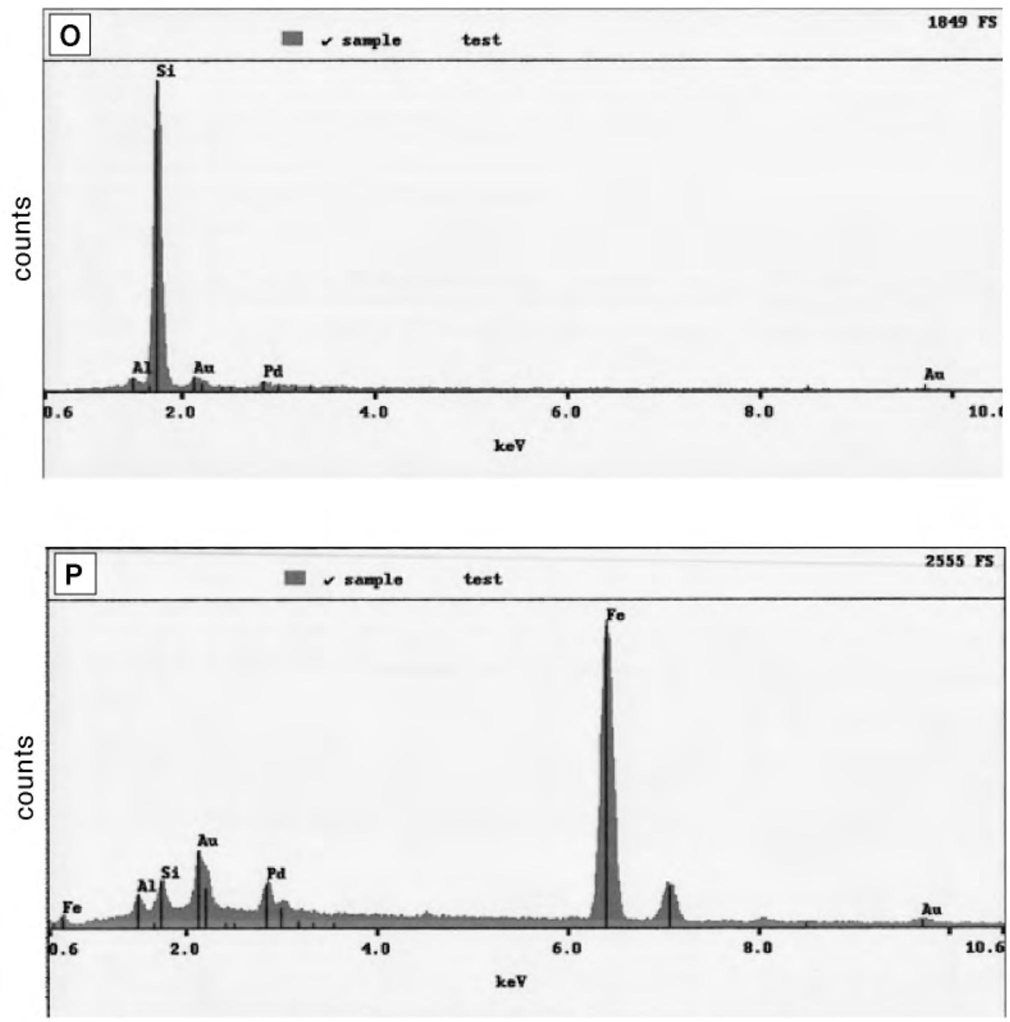

Attachment 7. EDS spectrum showing relative elemental composition of particles marked in Attachment 4. X-axis shows energy level, y-axis represents counts. The samples were coated with Au/Pd.

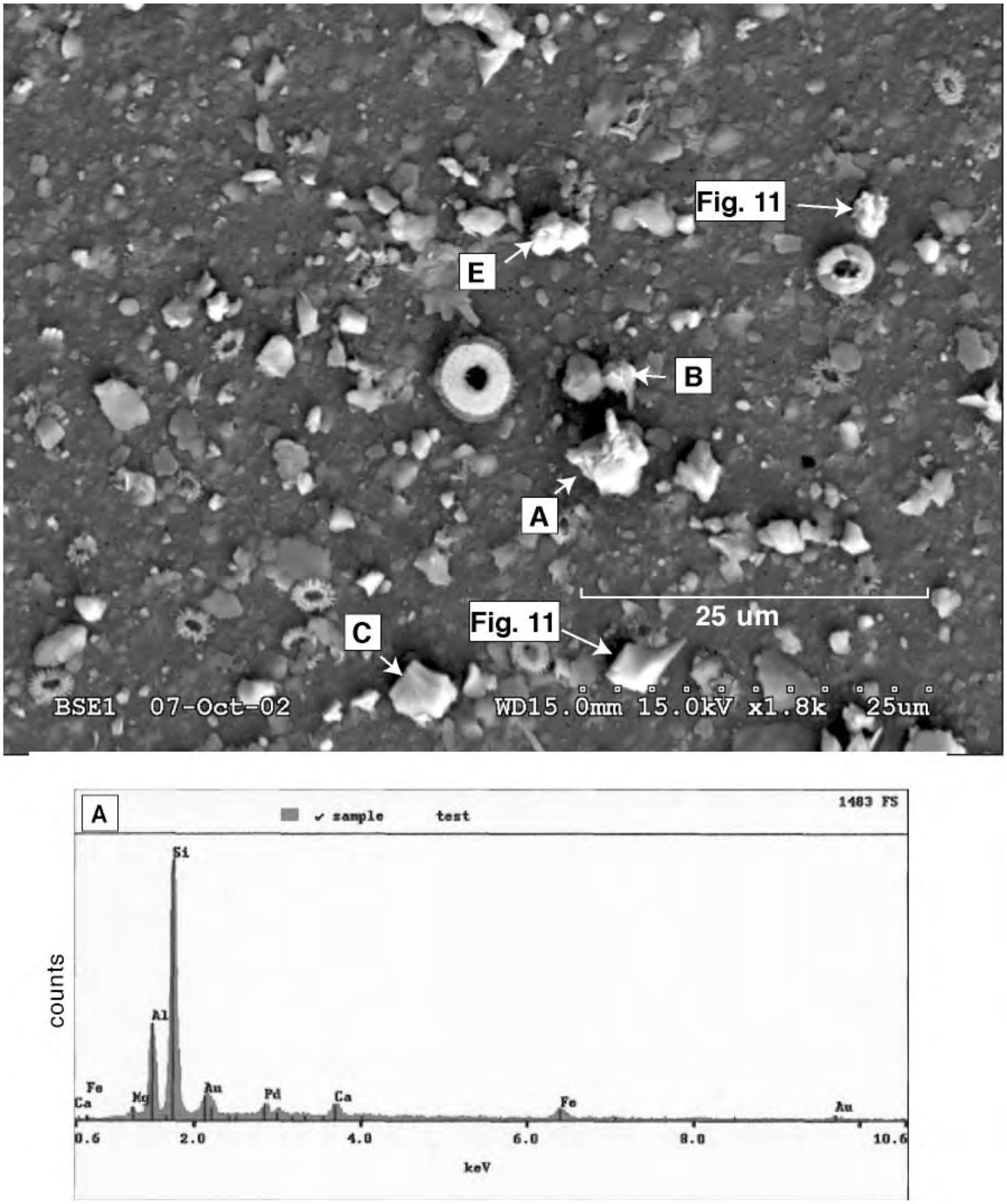

Attachment 8. Top: SEM images of a <6-phi sample from box core MD02-2553 (Pigmy Basin). Letters mark particles that have been analyzed using EDS, results shown in subsequent attachments. Bottom: EDS spectrum showing relative elemental composition of particle "A" marked in the above image. X-axis shows energy level, y-axis represents counts. The samples were coated with Au/Pd.

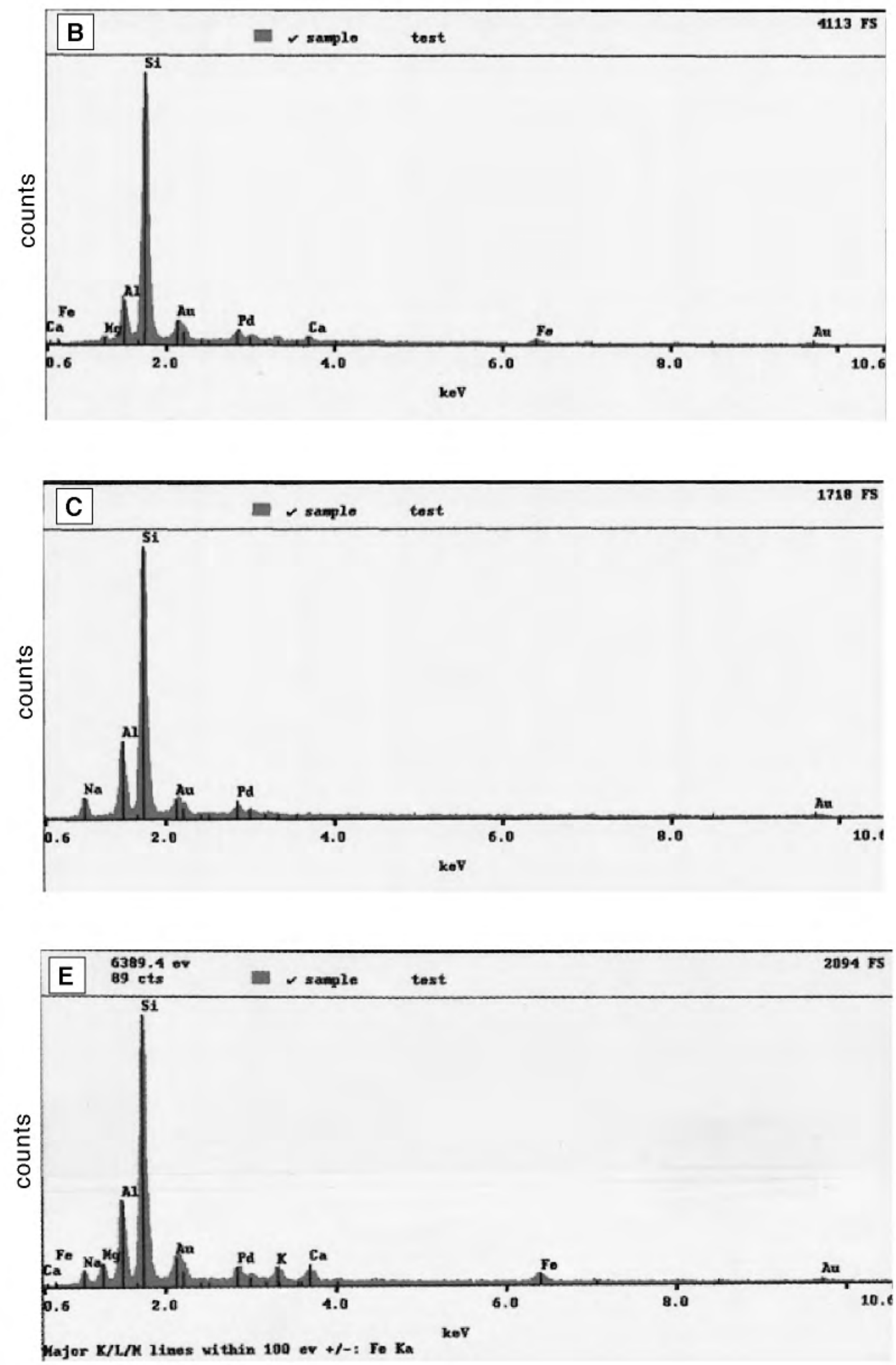

Attachment 9. EDS spectrum showing relative elemental composition of particles marked in Attachment 8. X-axis shows energy level, y-axis represents counts. The samples were coated with Au/Pd.

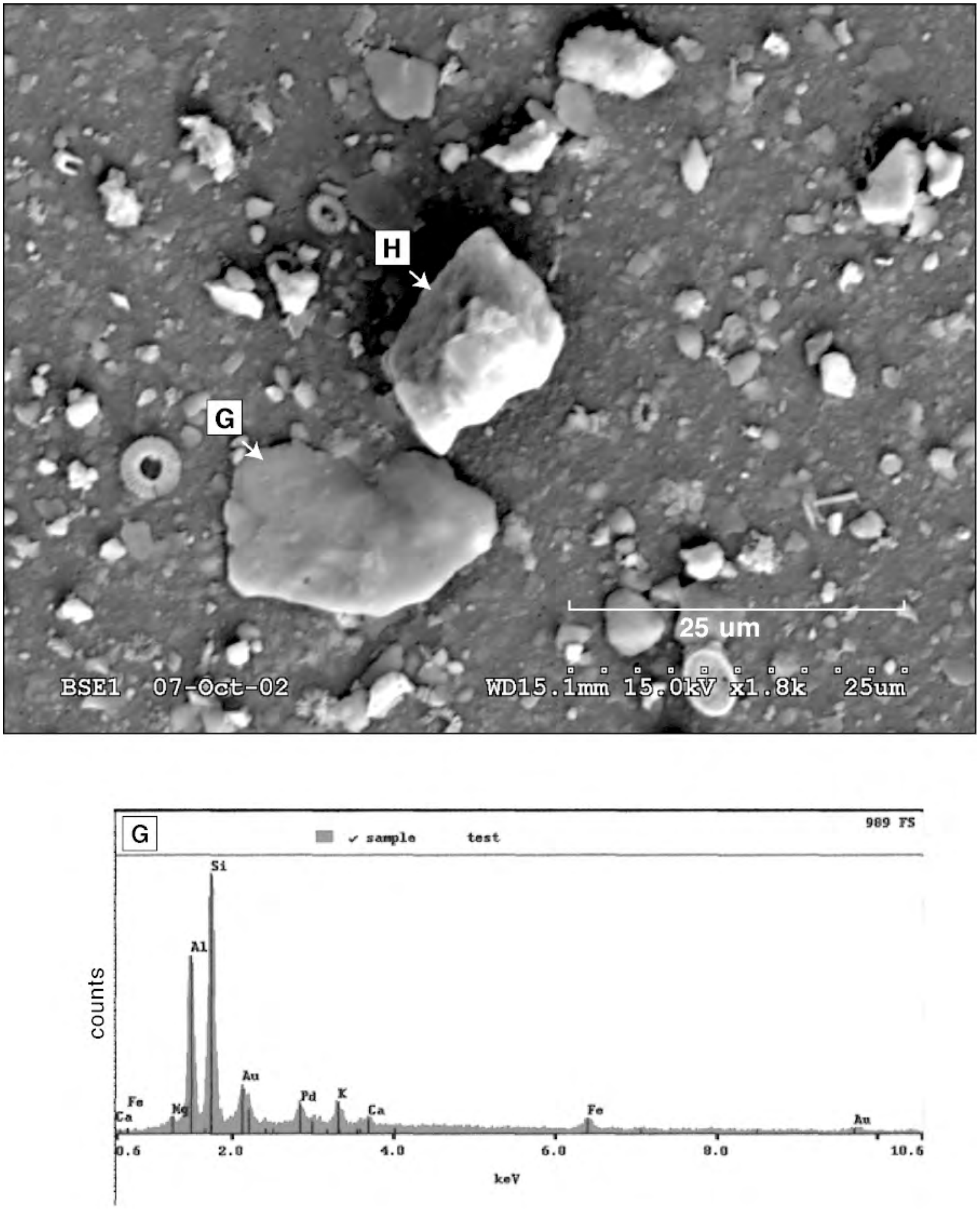

Attachment 10. Top: SEM images of a <6-phi sample from box core MD02-2553 (Pigmy Basin). Letters mark particles that have been analyzed using EDS, results shown in subsequent attachments. Bottom: EDS spectrum showing relative elemental composition of particle "G" marked in the above image. X-axis shows energy level, y-axis represents counts. The sample was coated with Au/Pd.

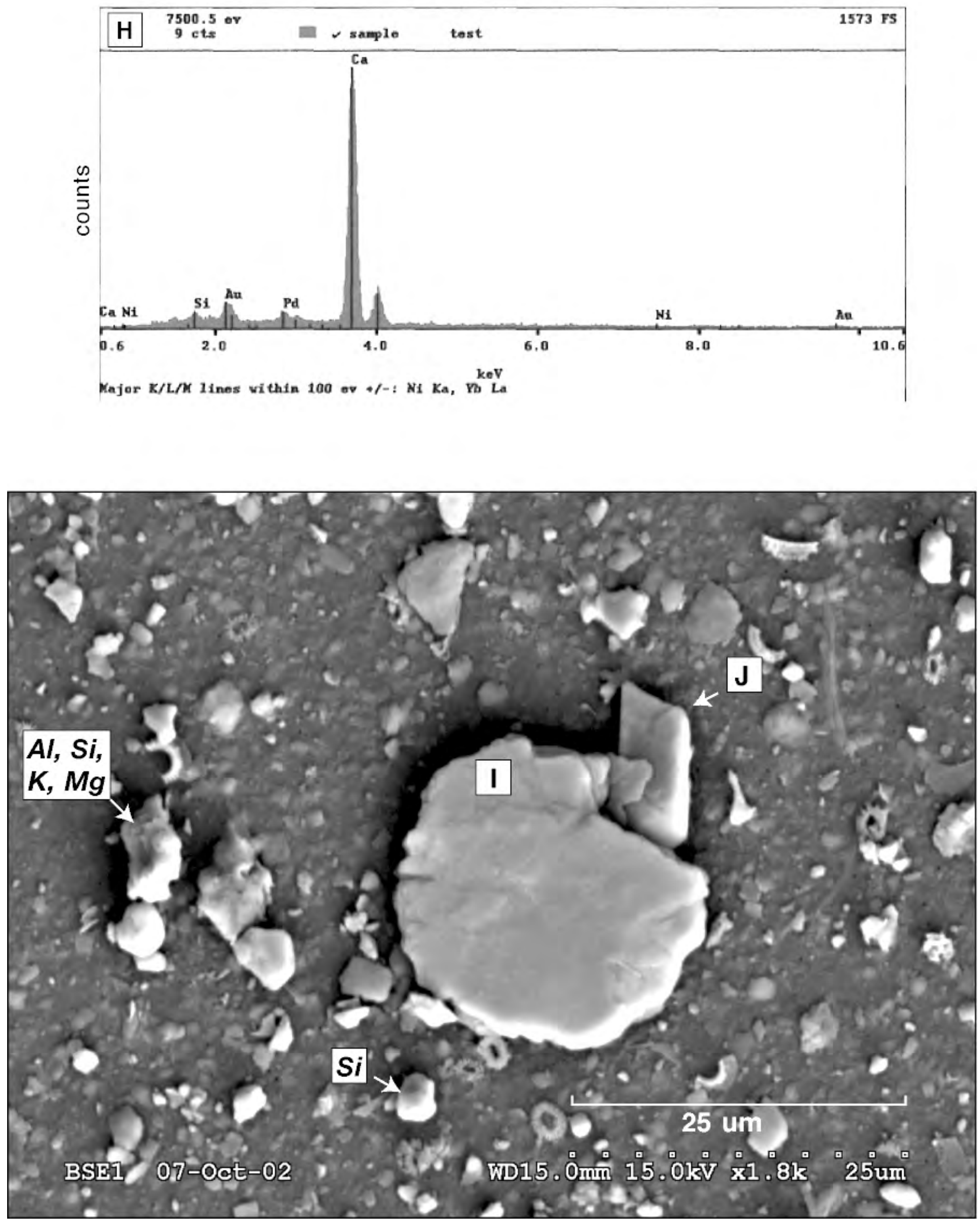

Attachment 11. Top: EDS spectrum showing relative elemental composition of particle "H" marked in Attachment 10. X-axis shows energy level, y-axis represents counts. The sample was coated with Au/Pd. Bottom: SEM images of a <6-phi sample from box core MD02-2553 (Pigmy Basin). Letters mark particles that have been analyzed using EDS, results shown in subsequent attachments. Italicized letters list element (Si = silicon, Al = aluminum, etc.) found within particle.

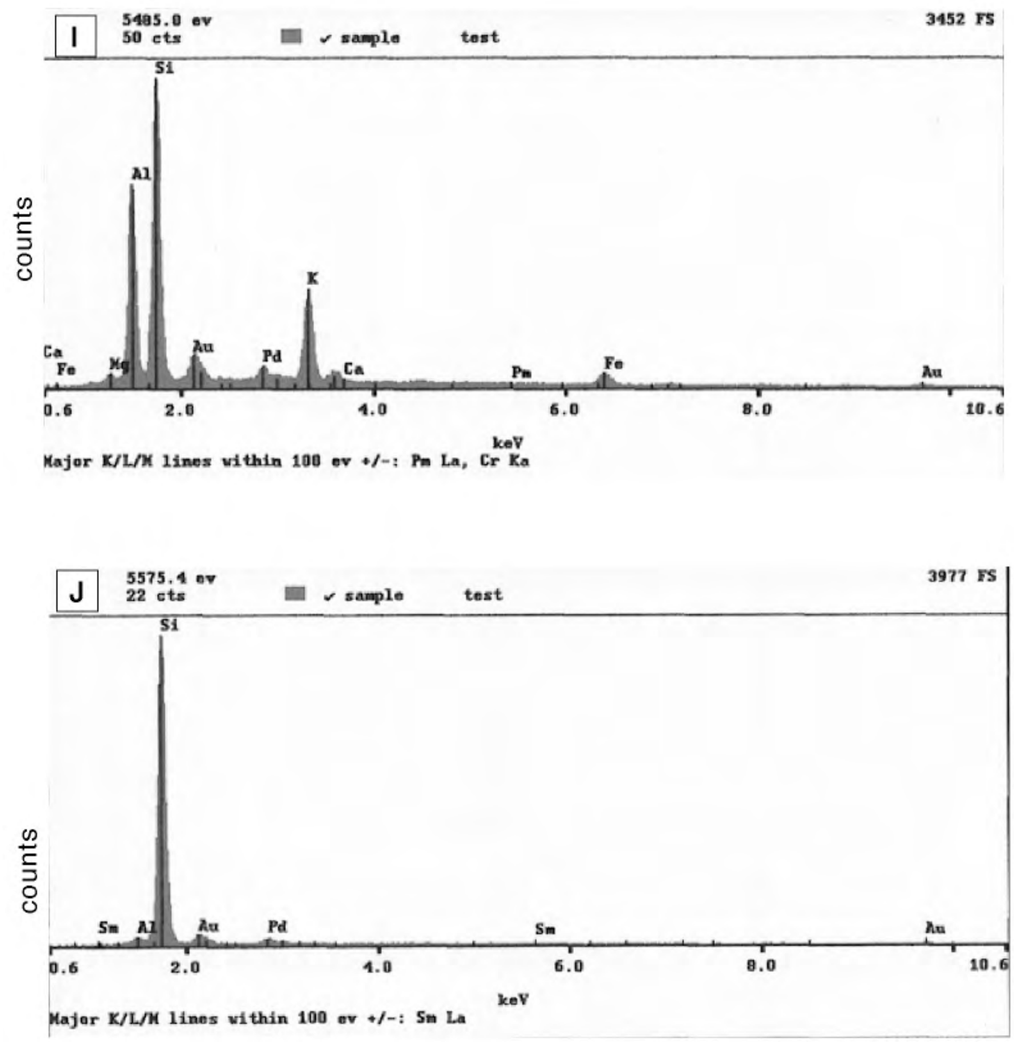

Attachment 12. EDS spectrum showing relative elemental composition of particles marked in Attachment 11. X-axis shows energy level, y-axis represents counts. The samples were coated with Au/Pd.

Attachment 13. Downcore chemical analysis of the top 2 m of box core MD02-2550 (Orca Basin). Measured using ICP-OES. Attachment 14 includes certification analysis for these data.

REPORT 25582 CODE 1F-TOTAL DIGESTION ICP																								
SAMPLE	Depth	Ag	Cd	Cu	Mn	Mo	Ni	Pb	Zn	Al	Be	Bi	Ca	Co	Fe	K	Mg	Na	P	Sr	Ti	V	Y	S
NUMBER	cm	ppm	ppm	ppm	ppm	ppm	ppm	ppm	ppm	%	ppm	ppm	%	ppm	%	%	%	%	%	ppm	%	ppm	ppm	%
MD02-2550 0-2	1	-0.3	-0.3	22	547	4	28	13	48	2.51	1	-2	4.78	6	1.81	1.04	0.90	13.59	0.036	254	0.16	73	11	0.515
MD02-2550 0-2 /R	1	-0.3	-0.3	21	567	3	26	15	49	2.81	1	-2	4.92	6	1.89	1.10	0.96	14.16	0.037	261	0.16	76	12	0.534
MD02-2550 2-4A	3	-0.3	-0.3	23	579	3	27	16	48	2.85	1	-2	5.09	6	1.98	1.15	0.99	13.32	0.033	273	0.16	82	12	0.486
MD02-2550 2-4B	3	-0.3	-0.3	23	613	3	33	20	53	2.99	1	-2	5.27	7	2.15	1.15	0.99	13.20	0.035	282	0.17	82	13	0.515
MD02-2550 2-4C	3	-0.3	-0.3	21	581	2	26	14	45	2.79	1	-2	4.99	5	1.98	1.12	0.96	13.12	0.033	263	0.17	79	12	0.479
MD02-2550 8-10	9	-0.3	-0.3	22	650	5	30	16	48	2.73	1	-2	5.10	7	1.99	1.08	0.96	13.49	0.034	268	0.16	75	11	0.545
MD02-2550 20-22	21	-0.3	-0.3	20	578	2	22	15	48	2.52	1	-2	4.86	6	1.73	1.05	0.91	13.71	0.033	262	0.16	74	11	0.464
MD02-2550 30-32	31	-0.3	-0.3	21	613	1	21	18	46	2.76	1	-2	4.78	6	1.91	1.12	1.03	13.48	0.034	258	0.17	79	12	0.492
MD02-2550 40-42	41	-0.3	-0.3	21	553	-1	19	10	45	2.67	1	-2	4.80	6	1.70	1.09	0.94	13.80	0.035	257	0.16	74	11	0.567
MD02-2550 50-52	51	-0.3	-0.3	20	492	2	20	12	43	2.64	1	-2	4.75	6	1.86	1.08	0.93	13.99	0.031	255	0.16	72	11	0.560
MD02-2550 60-62	61	-0.3	-0.3	22	503	2	23	14	49	2.46	1	-2	5.02	6	1.98	1.11	0.94	12.98	0.035	267	0.17	78	11	0.585
MD02-2550 70-72	71	-0.3	-0.3	19	447	1	18	12	44	2.31	1	-2	4.40	5	1.91	1.02	0.81	14.41	0.034	234	0.15	69	10	0.856
MD02-2550 80-82	81	-0.3	-0.3	22	539	-1	21	13	48	3.55	1	-2	4.73	6	1.83	1.22	1.04	13.03	0.033	251	0.18	82	13	0.444
MD02-2550 90-92	91	-0.3	-0.3	20	539	-1	20	12	43	2.35	1	-2	5.39	5	1.70	1.02	0.85	13.16	0.033	278	0.15	71	11	0.572
MD02-2550 100-102	101	-0.3	-0.3	22	510	2	22	18	48	3.52	1	-2	4.98	6	1.83	1.19	1.07	12.31	0.035	262	0.18	80	12	0.546
MD02-2550 110-112	111	-0.3	-0.3	21	451	1	21	14	46	2.63	1	-2	4.52	6	1.85	1.11	0.90	13.61	0.033	247	0.16	76	11	0.580
MD02-2550 120-122	121	-0.3	-0.3	21	487	1	21	15	45	2.48	1	-2	4.89	5	1.94	1.11	0.96	13.68	0.032	262	0.16	76	11	0.517
MD02-2550 130-132	131	-0.3	-0.3	20	464	-1	20	13	45	2.21	1	-2	4.87	5	1.88	1.04	0.91	14.15	0.030	252	0.15	69	11	0.770
MD02-2550 140-142	141	-0.3	-0.3	23	1319	2	24	16	52	3.11	1	-2	5.69	7	2.06	1.24	1.09	12.11	0.040	287	0.19	96	14	0.601
MD02-2550 150-152	151	-0.3	-0.3	20	552	1	21	11	48	2.53	2	-2	5.16	6	1.99	1.26	1.09	12.16	0.032	248	0.18	80	12	0.599
MD02-2550 160-162	161	-0.3	-0.3	21	766	10	23	18	50	2.22	1	-2	5.23	8	1.98	1.17	0.99	13.05	0.034	262	0.17	85	11	0.724
MD02-2550 170-172	171	-0.3	-0.3	22	984	2	23	16	51	4.36	1	-2	6.29	7	2.23	1.34	1.30	11.42	0.039	286	0.20	90	15	0.760
MD02-2550 180-182	181	-0.3	-0.3	20	480	2	19	9	45	2.53	1	-2	4.91	6	1.83	1.07	0.90	11.72	0.030	255	0.16	74	11	0.615
MD02-2550 180-182/R	181	-0.3	-0.3	19	455	3	19	14	43	2.68	1	-2	4.62	5	1.76	1.04	0.85	11.89	0.031	239	0.16	70	11	0.604
MD02-2550 190-192	191	-0.3	-0.3	21	496	5	32	13	51	3.40	1	-2	5.05	8	1.86	1.25	1.04	12.46	0.030	250	0.18	81	12	0.512
MD02-2550 198-200	199	-0.3	-0.3	24	570	2	23	22	57	3.62	1	-2	5.16	7	2.23	1.34	1.10	10.71	0.033	253	0.20	89	14	0.770

Attachment 14. Downcore chemical analysis of the top 2 m of box core MD02-2553 (Pigmy Basin). Measured using ICP-OES. Table includes certification analysis and notifications.

REPORT 25582 CODE 1F-TOTAL DIGESTION ICP																							
SAMPLE	Depth	Ag	Cd	Cu	Mn	Mo	Ni	Pb	Zn	Al	Be	Bi	Ca	Co	Fe	K	Mg	Na	P	Sr	Ti	V	Y	S
NUMBER	cm	ppm	ppm	ppm	ppm	ppm	ppm	ppm	ppm	%	ppm	ppm	%	ppm	%	%	%	%	%	ppm	%	ppm	ppm	%
MD02-2553 0-2	1.5	-0.3	-0.3	44	3360	5	40	19	96	6.65	2	-2	7.61	12	3.55	2.06	1.77	2.67	0.051	408	0.34	131	22	0.215
MD02-2553 10-12	11	-0.3	-0.3	40	3394	2	38	19	93	8.86	3	-2	6.95	14	3.68	2.32	2.18	2.56	0.062	368	0.37	134	31	0.225
MD02-2553 20-22	21	-0.3	-0.3	41	823	-1	32	17	92	10.37	3	-2	7.93	9	3.76	2.25	1.99	2.61	0.059	438	0.39	140	37	0.250
MD02-2553 30-32	31	-0.3	-0.3	43	883	-1	35	19	89	9.43	3	-2	7.58	10	4.20	2.47	2.22	2.76	0.059	399	0.37	139	32	0.281
MD02-2553 40-42	41	-0.3	-0.3	39	974	-1	32	17	90	10.11	3	-2	8.56	10	3.47	2.55	2.25	2.71	0.057	439	0.37	139	35	0.288
MD02-2553 50-52	51	-0.3	-0.3	41	1348	2	38	15	93	5.64	3	-2	5.34	12	4.56	2.39	2.24	2.30	0.053	254	0.39	142	25	0.200
MD02-2553 60-62	61	-0.3	-0.3	36	1305	-1	39	20	91	5.41	3	-2	6.11	14	3.82	2.41	2.28	2.42	0.049	273	0.39	140	24	0.290
MD02-2553 70-72	71	-0.3	-0.3	30	3215	-1	35	14	89	4.78	2	-2	6.28	11	3.77	2.08	1.78	2.55	0.050	341	0.35	140	21	0.182
MD02-2553 70-72/R	71	-0.3	-0.3	32	3181	-1	35	16	91	4.88	2	-2	6.41	11	3.71	2.10	1.81	2.38	0.051	344	0.35	144	22	0.169
MD02-2553 80-82	81	-0.3	-0.3	39	1355	-1	33	16	85	10.18	2	-2	8.21	10	3.46	2.40	2.02	2.24	0.057	434	0.35	136	32	0.209
MD02-2553 90-92	91	-0.3	-0.3	39	1201	-1	41	16	85	8.53	2	-2	7.75	15	3.67	2.27	1.96	2.42	0.057	422	0.34	140	29	0.229
MD02-2553 100-102	101	-0.3	-0.3	40	1129	-1	35	15	88	10.23	3	-2	8.27	11	3.59	2.36	2.11	2.22	0.059	435	0.37	138	37	0.213
MD02-2553 110-112	111	-0.3	-0.3	35	973	-1	32	16	84	6.33	2	-2	8.00	9	3.47	2.05	1.68	2.07	0.053	411	0.34	132	26	0.167
MD02-2553 120-122	121	-0.3	-0.3	39	1056	-1	32	16	87	9.17	3	-2	5.93	11	3.93	2.56	2.28	2.11	0.054	285	0.40	142	32	0.165
MD02-2553 130-132	131	-0.3	-0.3	32	1352	-1	32	13	83	9.58	2	-2	6.57	10	3.52	2.56	2.46	2.05	0.054	279	0.38	129	34	0.177
MD02-2553 140-142	141	-0.3	0.3	34	1338	2	33	16	88	9.37	3	-2	6.85	9	3.45	2.52	2.26	2.14	0.061	337	0.36	139	35	0.207
MD02-2553 150-152	151	-0.3	-0.3	35	1247	-1	33	17	91	8.23	3	-2	6.56	9	3.31	2.35	1.91	2.05	0.054	341	0.34	145	29	0.209
MD02-2553 160-162	161	-0.3	-0.3	28	1727	1	38	10	86	4.89	2	-2	5.74	11	3.68	2.14	1.87	2.04	0.050	287	0.34	135	21	0.162
MD02-2553 170-172	171	-0.3	-0.3	31	1089	3	34	14	93	8.35	3	-2	6.69	12	3.57	2.35	2.01	2.03	0.056	342	0.34	137	29	0.182
MD02-2553 180-182	181	-0.3	-0.3	42	1024	-1	37	15	90	7.30	2	-2	7.05	11	3.49	2.31	2.01	2.09	0.053	348	0.33	139	26	0.233
MD02-2553 190-192	191	-0.3	-0.3	31	1004	1	34	16	86	8.51	2	-2	6.37	11	3.44	2.44	2.25	1.84	0.055	292	0.34	130	30	0.183
MD02-2553 200-202	201	-0.3	-0.3	37	1044	2	38	21	85	8.84	2	-2	5.77	11	3.44	2.51	2.34	1.70	0.051	234	0.36	128	31	0.288
STANDARDS:																								
AL-1			0.03	3	31	0.1	2	4.5	8	9.841	2.7	0.03	0.274	0.2	0.052	0.116	0.021	7.856	0.016	80	0.007	2	6.8	0.0085
AL-I		-0.3	-0.3	2	16	2	-1	5	7	12.34	3	-2	0.37	-1	0.06	0.12	0.03	6.52	0.014	89	-0.01	-2	4	0.022
SDC-1 cert		0.041	(.08	30	883	(.25	38	25	103	8.338	3.0	0.26	1.001	17.9	4.825	2.722	1.019	1.521	0.069	183	0.606	102	40	0.065
SDC-1		-0.3	-0.3	44	963	2	33	20	99	6.53	4	-2	1.04	15	4.75	2.73	1.10	1.48	0.050	168	0.62	99	36	0.075
DNC-1 cert		(.027	(.182	96	1154	(.7	247	6.3	66	9.687	1	(.02	8.055	54.7	6.94	0.19	6.06	1.39	0.037	145	0.287	148	18	(0.039
DNC-1		-0.3	-0.3	107	1243	-1	277	8	64	7.75	-1	-2	8.45	51	7.26	0.18	6.93	1.53	0.023	144	0.31	157	20	0.079
SCO-1 cert		0.134	0.14	28.7	410	1.37	27	31	103	7.24	1.84	0.37	1.87	10.5	3.59	2.30	1.64	0.67	0.090	174	0.38	131	26	0.063
SCO-1		-0.3	-0.3	29	409	3	26	28	99	5.07	2	-2	1.85	9	3.37	2.14	1.67	0.65	0.066	152	0.35	130	21	0.075
GXR-6 cert		1.3	(1	66	1008	2.4	27	101	118	17.68	1.4	(.29	0.179	13.8	5.58	1.87	0.61	0.1	0.035	35	0.498	186	14	0.016
GXR-6		0.5	-0.3	67	1151	4	18	103	120	15.95	2	-2	0.28	7	5.36	2.38	1.04	0.12	0.045	57	0.53	182	24	0.017
GXR-2 cert		17	4.1	76	1008	(2.1	21	690	530	16.46	1.7	(.69	0.929	8.6	1.86	1.37	0.85	0.56	0.105	160	0.3	52	17	0.031
GXR-2		15.9	3.1	78	813	3	17	696	503	5.30	2	-2	0.68	7	1.66	1.15	0.65	0.50	0.045	121	0.29	51	9	0.024
GXR-1 cert		31	3.3	1110	853	18	41	730	760	3.52	1.22	1380	0.958	8.2	23.64	0.05	0.22	0.05	0.065	275	0.036	80	32	0.257
GXR-1		31.2	2.5	1201	967	23	39	798	722	1.38	1	1168	0.90	3	24.36	0.04	0.20	0.05	0.048	291	0.02	85	38	0.292
GXR-4 cert		4	(.86	6520	155	310	42	52	73	7.20	1.9	19	1.01	14.6	3.09	4.01	1.66	0.56	0.120	221	0.29	87	14	1.770
GXR-4		3.0	-0.3	6044	153	311	38	46	69	4.63	2	17	1.00	11	2.76	3.85	1.81	0.48	0.096	204	0.21	82	15	1.895
Note: Certificate data underlined are recommended values; other values are proposed except those preceded by a "(" which are information values.																								
Barite, gahnite, chromite, cassiterite, zircon, sphene, magnetite, and sulphates may not be totally dissolved.																								
Aluminium and Yttrium may only be paritally extracted.																								
Sulphur associated with barite will not be extracted. Rutile, ilmenite and monazite may not be fully extracted.																								

Attachment 15. Downcore grain-size analysis of box core MD02-2550 (Orca Basin), measured using laser diffraction. Depth is to midpoint of 2-cm interval. Mean values are in phi.

Grainsize_DataTable		% finer than										
Sample I.D.	Depth mdpt (m)	5%	10%	16%	25%	50%	75%	84%	90%	95%	Inman Mean	Sorting Value
2550-000-002	0.020	10.284	9.752	9.247	8.674	7.610	6.624	6.123	5.610	4.336	7.685	1.532
2550-008-010	0.090	9.837	9.103	8.555	8.029	7.059	6.159	5.728	5.287	4.487	7.142	1.371
2550-020-022	0.210	10.204	9.655	9.171	8.651	7.694	6.834	6.426	6.030	5.467	7.798	1.310
2550-040-042	0.410	10.414	9.951	9.506	8.977	7.985	7.155	6.790	6.460	6.019	8.148	1.259
2550-050-052	0.510	10.091	9.434	8.857	8.273	7.207	6.144	5.549	4.654	2.743	7.203	1.809
2550-052-054	0.530	10.010	9.352	8.784	8.183	6.944	5.318	4.342	3.496	2.776	6.563	2.343
2550-060-062	0.610	10.185	9.614	9.106	8.566	7.577	6.667	6.210	5.745	4.689	7.658	1.411
2550-070-072	0.710	10.375	9.886	9.410	8.855	7.828	6.911	6.441	5.916	4.131	7.925	1.469
2550-080-082	0.810	10.410	9.939	9.475	8.912	7.835	6.847	6.309	5.685	3.369	7.892	1.614
2550-090-092	0.910	10.430	9.989	9.578	9.093	8.130	7.222	6.706	6.023	4.631	8.142	1.535
2550-100-102	1.010	10.727	10.414	10.108	9.703	8.751	7.891	7.502	7.105	6.102	8.805	1.299
2550-106-108	1.070	10.155	9.569	9.039	8.461	7.356	6.169	5.459	4.592	3.237	7.249	1.935
2550-110-112	1.110	10.422	9.949	9.475	8.896	7.832	6.924	6.476	6.014	5.167	7.976	1.441
2550-120-122	1.210	10.281	9.732	9.207	8.623	7.579	6.648	6.194	5.762	4.929	7.700	1.431
2550-126-128	1.270	10.317	9.782	9.244	8.608	7.412	6.199	5.565	4.882	3.861	7.404	1.863
2550-140-142	1.410	10.526	10.119	9.717	9.212	8.214	7.404	7.058	6.750	6.345	8.388	1.231
2550-160-162	1.610	10.129	9.521	8.977	8.401	7.337	6.322	5.817	5.319	4.520	7.397	1.541
2550-170-172	1.710	10.398	9.908	9.412	8.812	7.711	6.759	6.325	5.960	5.547	7.869	1.426
2550-180-182	1.810	10.446	9.996	9.553	9.010	7.960	7.040	6.583	6.122	5.503	8.068	1.444
2550-198-200	1.990	10.402	9.923	9.446	8.863	7.740	6.664	6.101	5.570	4.705	7.773	1.646
2550-210-212	2.110	10.520	10.102	9.682	9.149	8.106	7.252	6.867	6.512	6.008	8.275	1.318
2550-230-232	2.310	10.418	9.956	9.506	8.959	7.856	6.597	5.533	4.007	2.795	7.520	2.476
2550-240-242	2.410	10.442	9.992	9.551	9.013	7.957	6.969	6.412	5.797	4.756	7.982	1.608
2550-250-252	2.510	10.501	10.081	9.667	9.147	8.059	6.921	5.974	4.434	2.763	7.821	2.357
2550-254-256	2.550	10.350	9.857	9.380	8.807	7.631	6.145	5.183	4.280	3.270	7.281	2.264
2550-260-262	2.610	10.416	9.964	9.534	9.010	7.951	6.920	6.346	5.774	4.853	7.940	1.618
2550-270-272	2.710	10.637	10.282	9.934	9.483	8.520	7.742	7.419	7.144	6.797	8.677	1.169
2550-280-282	2.810	10.605	10.231	9.856	9.363	8.321	7.433	7.004	6.544	5.680	8.430	1.410
2550-290-292	2.910	10.514	10.094	9.675	9.140	8.055	7.094	6.594	6.061	5.231	8.135	1.540
2550-300-302	3.010	10.581	10.193	9.806	9.295	8.222	7.321	6.887	6.414	5.395	8.346	1.441

Attachment 16. Downcore grain-size analysis of boxcore MD02-2553 (Pigmy Basin), measured using laser diffraction. Depth is to midpoint of 2-cm interval. Mean values are in phi.

Grainsize_DataTable		% finer than										
Sample I.D.	Depth mdpt (m)	5%	10%	16%	25%	50%	75%	84%	90%	95%	Inman Mean	Sorting Value
2553-000-002	0.010	10.377	9.871	9.340	8.667	7.414	6.288	5.739	5.134	3.997	7.540	1.766
2553-010-012	0.110	10.422	9.943	9.437	8.770	7.460	6.149	5.362	4.337	3.166	7.400	2.217
2553-014-016	0.150	10.576	10.192	9.811	9.319	8.282	7.396	6.982	6.564	5.895	8.397	1.377
2553-016-018	0.170	10.507	10.083	9.651	9.085	7.919	6.866	6.335	5.852	5.195	7.993	1.617
2553-020-022	0.210	10.637	10.275	9.911	9.404	8.269	7.345	6.921	6.499	5.908	8.416	1.453
2553-028-030	0.290	10.539	10.139	9.748	9.248	8.221	7.372	6.997	6.655	6.145	8.373	1.296
2553-030-032	0.310	10.493	10.052	9.589	8.966	7.704	6.497	5.774	4.790	3.179	7.682	2.088
2553-040-042	0.410	10.503	10.074	9.636	9.050	7.835	6.698	6.066	5.400	3.872	7.851	1.825
2553-044-046	0.450	10.544	10.144	9.749	9.237	8.156	7.219	6.764	6.297	5.655	8.256	1.470
2553-050-052	0.510	10.679	10.341	10.001	9.530	8.365	7.337	6.836	6.329	5.762	8.419	1.600
2553-060-062	0.610	10.628	10.263	9.897	9.388	8.170	7.056	6.495	6.007	5.437	8.196	1.690
2553-070-072	0.710	10.557	10.150	9.725	9.139	7.862	6.552	5.837	5.138	3.796	7.781	2.000
2553-080-082	0.810	10.583	10.199	9.814	9.292	8.094	6.958	6.336	5.774	5.076	8.075	1.759
2553-090-092	0.910	10.557	10.152	9.737	9.168	7.917	6.644	5.823	4.788	3.291	7.780	2.190
2553-100-102	1.010	10.651	10.293	9.934	9.433	8.252	7.160	6.527	5.913	5.250	8.231	1.760
2553-110-112	1.110	10.623	10.263	9.904	9.416	8.250	7.157	6.568	6.013	5.542	8.236	1.702
2553-120-122	1.210	10.623	10.261	9.900	9.400	8.172	6.978	6.332	5.802	5.270	8.116	1.799
2553-130-132	1.310	10.565	10.173	9.777	9.245	8.073	7.000	6.459	5.983	5.425	8.118	1.631
2553-140-142	1.410	10.630	10.263	9.895	9.380	8.160	7.067	6.484	5.959	5.341	8.190	1.711
2553-150-152	1.510	10.710	10.389	10.066	9.619	8.461	7.425	6.941	6.450	5.872	8.503	1.584
2553-160-162	1.610	10.686	10.352	10.020	9.562	8.436	7.439	6.981	6.526	5.941	8.500	1.518
2553-170-172	1.710	10.570	10.180	9.793	9.274	8.117	7.054	6.488	5.929	5.298	8.141	1.672
2553-180-182	1.810	10.583	10.197	9.809	9.281	8.087	6.963	6.339	5.758	5.042	8.074	1.761
2553-182-184	1.830	10.632	10.277	9.929	9.472	8.470	7.651	7.307	6.997	6.540	8.618	1.237
2553-190-192	1.910	10.703	10.383	10.070	9.657	8.632	7.700	7.317	6.987	6.582	8.694	1.335
2553-198-200	1.990	10.691	10.360	10.032	9.587	8.546	7.641	7.237	6.840	6.226	8.635	1.374
2553-200-202	2.010	10.805	10.529	10.257	9.891	8.919	8.048	7.737	7.510	7.290	8.997	1.191
2553-210-212	2.110	10.621	10.249	9.870	9.340	8.130	7.010	6.376	5.763	4.630	8.123	1.788
2553-220-222	2.210	10.644	10.284	9.920	9.410	8.162	6.925	6.200	5.563	4.446	8.060	1.924
2553-230-232	2.310	10.635	10.272	9.901	9.377	8.113	6.894	6.202	5.598	4.214	8.052	1.890
2553-240-242	2.410	10.614	10.242	9.865	9.359	8.230	7.196	6.635	6.086	5.439	8.250	1.636
2553-250-252	2.510	10.574	10.187	9.797	9.272	8.062	6.764	5.830	4.526	2.844	7.814	2.373
2553-260-262	2.610	10.592	10.207	9.817	9.282	8.057	6.808	5.998	5.171	3.517	7.907	2.056
2553-270-272	2.710	10.658	10.308	9.960	9.481	8.317	7.221	6.590	5.980	5.370	8.275	1.751
2553-280-282	2.810	10.693	10.358	10.020	9.546	8.386	7.323	6.722	6.044	5.059	8.371	1.751
2553-290-292	2.910	10.610	10.238	9.865	9.361	8.192	7.103	6.500	5.882	4.966	8.183	1.740
2553-300-302	3.010	10.669	10.324	9.976	9.491	8.322	7.278	6.744	6.206	5.602	8.360	1.643

Attachment 17. Texture analysis of cores MD02-2550 and MD02-2553, determined from grain-size analysis. Sand, silt, and clay refer to >4 phi, 4 – 8 phi, and <8 phi, respectively. Inman mean values are in phi.

Sample I.D.	depth (m)	Sand %	Silt %	Clay %	Inman mean	Inman sorting
2550-000-002	0.020	4.596	55.700	39.650	7.685	1.532
2550-008-010	0.090	3.945	70.570	25.500	7.142	1.371
2550-020-022	0.210	1.622	57.420	41.030	7.798	1.310
2550-040-042	0.410	0.086	50.370	49.480	8.148	1.259
2550-050-052	0.510	8.085	61.400	30.470	7.203	1.809
2550-052-054	0.530	13.396	58.350	28.240	6.563	2.343
2550-060-062	0.610	4.025	57.890	38.100	7.658	1.411
2550-070-072	0.710	4.863	50.130	44.990	7.925	1.469
2550-080-082	0.810	5.560	48.900	45.540	7.892	1.614
2550-090-092	0.910	3.956	42.200	53.730	8.142	1.535
2550-100-102	1.010	0.917	27.110	71.940	8.805	1.299
2550-106-108	1.070	7.100	58.490	34.420	7.249	1.935
2550-110-112	1.110	3.085	51.680	45.270	7.976	1.441
2550-120-122	1.210	3.389	58.020	38.560	7.700	1.431
2550-126-128	1.270	5.436	57.990	36.490	7.404	1.863
2550-140-142	1.410	0.000	43.431	56.590	8.388	1.231
2550-160-162	1.610	3.657	63.230	33.270	7.397	1.541
2550-170-172	1.710	0.011	57.570	42.340	7.869	1.426
2550-180-182	1.810	0.129	51.000	48.810	8.068	1.444
2550-198-200	1.990	3.156	53.540	43.280	7.773	1.646
2550-210-212	2.110	0.261	46.680	53.080	8.275	1.318
2550-230-232	2.310	9.977	43.710	46.330	7.520	2.476
2550-240-242	2.410	3.509	47.670	48.760	7.982	1.608
2550-250-252	2.510	8.897	39.610	51.520	7.821	2.357
2550-254-256	2.550	8.435	49.960	41.580	7.281	2.264
2550-260-262	2.610	2.674	48.710	48.630	7.940	1.618
2550-270-272	2.710	0.000	33.320	66.730	8.677	1.169
2550-280-282	2.810	2.767	38.010	59.330	8.430	1.410
2550-290-292	2.910	2.003	46.470	51.460	8.135	1.540
2550-300-302	3.010	3.879	39.940	56.240	8.346	1.441

sample I.D.	depth (m)	Sand %	Silt %	Clay %	Inman mean	Inman sorting
2553-000-002	0.010	5.005	58.050	36.800	7.540	1.766
2553-010-012	0.110	8.524	52.990	38.400	7.400	2.217
2553-014-016	0.150	0.762	41.250	58.030	8.397	1.377
2553-016-018	0.170	1.483	50.580	47.950	7.993	1.617
2553-020-022	0.210	0.010	42.700	57.240	8.416	1.453
2553-028-030	0.290	0.004	43.496	56.520	8.373	1.296
2553-030-032	0.310	7.165	49.620	43.200	7.682	2.088
2553-040-042	0.410	5.265	48.710	46.030	7.851	1.825
2553-044-046	0.450	1.002	44.870	54.130	8.256	1.470
2553-050-052	0.510	0.000	41.022	58.910	8.419	1.600
2553-060-062	0.610	1.291	44.760	53.900	8.196	1.690
2553-070-072	0.710	5.518	47.570	46.790	7.781	2.000
2553-080-082	0.810	0.298	47.500	52.140	8.075	1.759
2553-090-092	0.910	7.181	44.710	47.980	7.780	2.190
2553-100-102	1.010	0.018	43.890	56.090	8.231	1.760
2553-110-112	1.110	0.000	43.984	55.980	8.236	1.702
2553-120-122	1.210	0.020	46.130	53.780	8.116	1.799
2553-130-132	1.310	0.227	47.970	51.700	8.118	1.631
2553-140-142	1.410	0.618	45.620	53.810	8.190	1.711
2553-150-152	1.510	0.000	38.716	61.270	8.503	1.584
2553-160-162	1.610	0.006	38.940	61.040	8.500	1.518
2553-170-172	1.710	0.331	46.830	52.900	8.141	1.672
2553-180-182	1.810	0.795	47.120	52.050	8.074	1.761
2553-182-184	1.830	0.000	35.680	64.410	8.618	1.237
2553-190-192	1.910	0.000	32.950	67.000	8.694	1.335
2553-198-200	1.990	0.001	34.730	65.170	8.635	1.374
2553-200-202	2.010	0.000	23.670	76.350	8.997	1.191
2553-210-212	2.110	3.664	43.260	53.090	8.123	1.788
2553-220-222	2.210	3.840	42.600	53.560	8.060	1.924
2553-230-232	2.310	4.664	42.860	52.430	8.052	1.890
2553-240-242	2.410	0.282	43.930	55.960	8.250	1.636
2553-250-252	2.510	8.316	40.220	51.430	7.814	2.373
2553-260-262	2.610	6.215	42.430	51.280	7.907	2.056
2553-270-272	2.710	0.015	42.480	57.620	8.275	1.751
2553-280-282	2.810	2.453	38.060	59.480	8.371	1.751
2553-290-292	2.910	1.399	43.890	54.630	8.183	1.740
2553-300-302	3.010	0.429	41.690	57.980	8.360	1.643